Lane Detection, Calibration, and Attitude Determination with a Multi-Layer Lidar for Vehicle Safety Systems

by

Jordan H. Britt

A thesis submitted to the Graduate Faculty of
Auburn University
in partial fulfillment of the
requirements for the Degree of
Master of Science

Auburn, Alabama
December 13, 2010

Keywords: lidar, calibration, attitude

Approved by:

John Hung Chair, Professor of Electrical and Computer Engineering
David Bevly Co-Chair, Professor of Mechanical Engineering
Thaddeus Roppel, Associate Professor of Electrical and Computer Engineering

Abstract

This thesis develops a lane detection algorithm which extracts lane markings from the road's surface in an effort to ascertain the lateral position of the vehicle in the lane using a lidar, with the goal of being incorporated into a larger lane departure warning system. The presented algorithm underwent numerous highway tests. These tests include both a comparison of the reported position of the algorithm using the lidar to a high accuracy global positioning system (GPS) as well tests more commonly found in literature. The results of which show that the presented algorithm is capable of determining its position in the lane to a high degree of accuracy and consistency.

Additionally, a novel lidar calibration method is developed which is capable of calibrating a 3D forward facing lidar mounted on a vehicle to a plane, through simply causing the vehicle to pitch. The presented algorithm will demonstrate the ability to determine vehicle attitude with sub degree accuracy. The algorithm is tested under a number of conditions ranging from in lab tests to on vehicle tests. During these test both attitude accuracy as well as processing time are analyzed. Finally, it is shown that this algorithm is capable of making highly accurate attitude calculations at a rate that is capable of running real-time.

Acknowledgments

I would like to acknowledge the help of my advisers Dr. David Bevly, Dr. John Hung, and Dr. Thaddeus Roppel for their advice, help, and oversight. I would also like to acknowledge the help of my parents, family, and friends, for your constant encouragement, rivalry, and support. Finally, I would like to thank all of my many lab mates, whose advice, help, and insight I have found invaluable and without which this project would be incomplete.

Table of Contents

List of Figures

List of Tables

Chapter 1

Introduction

Lane departure warning (LDW), also known as lane keeping assist (LKA), systems are vehicle safety systems inteded to alert the driver if the vehicle is drifting out of its intended lane of travel. The driver is alerted of lane departure by either an audible alert such as a tone, the sound of a rumble strip, or a haptic sensor such as a vibration of the steering wheel or driver's seat. These systems distinguish between intentional and unintentional lane departures, by whether the vehicle's turn signal has been engaged. As many as 52% of all highway fatalities in 2008 comprising almost 20,000 deaths occurred because of lane departure crashes, which was defined as "a non-intersection crash [that] occurs after a vehicle crosses an edge line or a center line, or otherwise leaves the traveled way [25]." Additionally, it has been recognized by the National Highway Traffic Safety Administration (NHTSA) that more fatalities than any other crash type occur due to single-vehicle road departure crashes [7]. NHTSA has also recognized the potential of technologies such as electronic stability control and LDW systems to save lives [7]. An additional driving hazard is vehicle rollover which has accounted for nearly 33% of all deaths from passenger vehicle crashes, and often has a disproportionately large ratio of accidents occurring to accidents which cause severe to fatal injuries when compared to other vehicular accident types [21, 17]. Vehicle rollover research is especially important considering that vehicles with higher centers of gravity such as trucks, vans, ans sport utility vehicles (SUV) are more prone to rollover and that their popularity is growing [19, 30, 31]. It is therefore of great interest to develop an effective LDW system as well as aid other vehicle safety systems such as rollover prevention and detection.

It is crucial to the development of a functional LDW system that a vehicle be able to accurately and consistently determine its position in a lane [13]. Currently, LDW systems utilize a combination of sensors to determine their position and attitude within a lane, namely a global positioning system (GPS), light detection and ranging (LiDAR) also known as a laser measurement system (LMS), cameras, and inertial navigation systems (INS) [22, 3]. GPS allows the user to determine the vehicle's global velocity and position, often to within a root mean square (rms) error of 10m to 30m [36, 16]. The INS utilizes gyroscopes and accelerometers to measure the rotation rate and acceleration of the vehicle [16]. Both the LiDAR and camera are used to detect lane markings and provide a position estimate of the vehicle's lateral position in the lane [29, 11]. However, as the vehicle undergoes various pitch and roll dynamics, errors can be introduced into both the lidar's and camera's measurements [14]. Additional measurement errors can be introduced by mounting and alignment errors, which typically consist of not properly aligning the lidar with either the vehicle's or other instrument's axes.

The lidar is a sensor that is similar in principle to both radio detection and ranging (radar) and sound detection and ranging (sonar), but instead of using electromagnetic waves such as in radar, or sound waves as in sonar, the lidar uses light to determine the distance between the lidar and some object. The lidar is able to determine the distance between itself and an object by transmitting a beam of light and then sensing the reflection of that same beam from an object. By measuring the time between transmission and reflection of this beam, the distance between the lidar and object can be determined. This technique is known as a time-of-flight (TOF) measurement. LiDAR is an ideal measurement sensor for LDW systems, because lidars are capable of quickly making dense, accurate, and precise distance and reflectivity measurements, often in three dimensions.

Many lidar systems used for LDW systems employ a host of different techniques for detecting and tracking lane markings. Lane markings are considered to be a visual queue for drivers to denote and separate lanes of travel, which typically take the form of either white or yellow, dashed or solid painted lines, as well as road surface reflectors or Botts' dots. However, signs, posts, rumble strips, and unpainted curbs, while having the potential to aid a driver in distinguishing the road's edge are not considered to be lane markings. The techniques used to detect lane markings regularly employ simple bounding, histograms, as well as more complicated vision processing techniques such as the Hough transform [23, 13, 26].

It is often necessary to calibrate a lidar so that it aligns with some common coordinate system, especially in the case of multi-sensor systems so that these sensors can be related to one another in a meaningful way [5]. Additionally this calibration process can help mitigate measurement errors, thus allowing the lidar algorithm to report more precise measurements. Calibration of the sensor in this sense, refers to finding the rigid body rotations that allow the lidar's coordinate frame to coincide with the vehicle's coordinate frame, as opposed to corresponding with another sensor's coordinate frame. Hence, the determination of the yaw, pitch, and roll of the lidar in reference to the vehicle's axes will constitute a calibrated lidar. Calibration techniques vary greatly, but often require the scanning of an object of known geometry [5, 27], a beacon or landmark [37, 32], or a planar surface [12, 38, 4, 28]. These calibration techniques additionally vary in how many degrees of freedom they calibrate to. Hence, whether they assume their lidar needs to be calibrated for only, pitch, roll, or yaw, as opposed to all three or some combination of the two. If a lidar is properly calibrated to the vehicle's axis, it has the additional functionality of being able to aid in the determination of the vehicle's attitude, which is of use in many safety systems, namely rollover prevention, because if the roll relative to the road can be determined with a lidar, then with the use of additional sensors, it can be determined what portion of vehicle roll is due to suspension deflection and what portion is due to road bank, thus facilitating the development of better rollover detection and prevention algorithms.

It is the focus of this thesis to develop an algorithm that is capable of tracking those lane markings previously mentioned with the goal of integrating those measurements into a lane departure warning system. Additionally this thesis will cover a method of lidar calibration and attitude estimation for correcting lidar misalignment as well as providing information of vehicle dynamics relative to a reference plane.

The thesis will first outline some background information on lidar based lane departure warning systems, as well as lidar based calibration and attitude determination techniques. It will then cover the specific algorithm and techniques used by the algorithm developed for lane detection as well as provide results for this algorithm. A method for lidar calibration and attitude estimation will then be covered, followed by testing and results of that calibration algorithm. Finally overall conclusions and future will work will be covered.

Chapter 2

Background

2.1 GPS/INS navigation background

Global Positioning Systems (GPS) have the ability to determine a users position accurately on the earth's surface. In contrast, inertial navigation systems (INS) utilize gyroscopes and accelerometers to determine a vehicle's rotation rate, acceleration, and velocity in a local coordinate frame. These two sensors are often combined in a Kalman filter to take advantage of each sensor's respective strengths. The strengths of an INS systems include fast update rates at the cost of unbounded error growth with time, while GPS has a relatively slow update rate but with bounded error [16]. This integration technique can often yield highly accurate position measurements. While both INS sensors and GPS receivers vary in quality, those found on commercial vehicles are typically poor, and lack the ability to be used for precise navigation for any appreciable amount of time [16]. However there are systems such as differential GPS (DGPS) that assist in eliminating GPS errors through the use of a base station with limited range, that allows for precise GPS positioning with decimeter accuracy, allowing for a "truth" solution of a vehicle's position to be obtained. It is worthwhile to note, that regardless of the accuracy of the integrated GPS/INS system, a map of the lanes must still be employed to determine the vehicle's position within the roadway; a limitation that a Light Detection and ranging (Lidar) system does not have. However a Lidar system cannot determine global position.

2.2 Lidar background

Light detection and ranging (Lidar) is a sensor technology which emits a focused beam of light (laser) and based on the returning beam, the distance between an object and the lidar can be calculated. The returning light that the lidar measures is known as backscatter. There are many different lidar technologies and techniques used for determining this distance. Some lidars known as continuous-wave lasers, look at the phase shift in the light beam itself, while others, often known as pulse lasers, simply count the time interval between transmission and reception [6]. The former is a more common type of lidar in the vehicle safety field, and is the type of lidar used in this thesis. Because a pulsed laser determines distance based on a time interval, there are several factors that affect the obtainable accuracy, precision, and range of a lidar system such as how fast the timer can operate, the maximum number of bits available to store a count, pulse rate, laser power, and detector sensitivity [6]. Typical lidars are capable of operating anywhere between 10Hz and 100Hz with accuracies in the decimeter and centimeter ranges. Some lidars operate in the visible spectrum, the vast majority of lidars do not. However some cameras have the ability to view the laser's beam contacting an object so that the lidar's scan can be visualized.

Lidars are further classified by how many dimensions (D) they are capable of measuring, and are divided into 1-D, 2-D, and 3-D. Lidars that measure a single distance, with no built in mechanism for moving the beam either horizontally or vertically are known as 1-D lidars, analogous to a laser-pointer that is capable of measuring distance only. Other lidar systems employ a rotating mirror such that the laser beam is swept horizontally similar to a fan shape; these are known as 2-D lidars and report both distance and the horizontal angle of the measurement. Other 3-D lidars either employ multiple lasers or a single laser or with the aid of a rotating mirror to make such common scan patterns as, horizontal sweeps at varying vertical angles, Z-shaped patterns, sinusoidal, and elliptical scans [6]. These 3-D lidars often adopt a polar coordinate system, and will report both the distance, horizontal angle, and vertical angle of the measurement.

Because the lidar system is actually transmitting a beam of light it is known as an active sensor, as opposed to a camera which would be a passive sensor. This often makes lidars more robust to changes in lighting, shadows, and environmental conditions, however a lidar scan is still capable of being "washed out" due to heavy precipitation. Additionally, despite being more resilient to change in lighting conditions than most cameras, direct sunlight can make it difficult to receive the reflected light, an error known as dazzling [24]. However, this is typically not an issue for LDW applications because the lidar is directed at the road and dazzling should only occur if the vehicle were cresting a steep hill. Finally, despite being able to make highly accurate measurements, lidars often do not take in as much environmental information as cameras, and therefore are often modeled as simply taking "slice" measurements of the environment the lidar is scanning.

In addition to measuring distance, some lidar systems are capable of measuring reflectivity, a measurement known as echo width. Reflectivity is often a function of distance from the lidar, as well as a function of the surface of the object measured. Hence, an object that is highly reflective at a large distance may return the same echo width measurement by the lidar as an object that is less reflective, but closer. This reflectivity measurement is often exploited by lane departure warning systems because often, lane markings are more reflective than the road's surface [23, 13, 24, 22, 26, 11].

2.3 Lane Departure warning background

One of the simpler methods of detecting lane markings is demonstrated in [23] which uses an Ibeo multilayer lidar. The lidar is mounted on the front of the vehicle and is contacting the ground at 10 to 30 m in front of the vehicle, and a region of interest (ROI) of approximately ±12 m in the lateral direction is established over which to process data, which is taken at a rate of 10 Hz at and at an angular resolution of 0.25° [23]. Due to the distance in front of the vehicle which is being scanned, the algorithm first begins with a preprocessing step in which vehicles must be distinguished from the road surface. Once this preprocessing is accomplished, those measurements not attributed to the road's surface are removed from consideration. The algorithm them attempts to determine the boundaries of the roadway (not lane markings) in an effort to determine the width and curvature of the roadway. The principle on which the lane extraction algorithm works is the idea that the lane marking's reflectivity is significantly more consistent than the road's reflectivity from a statistical point of view. Thus, the lane markings are extracted using a histogram, in which all lateral reflectivity measurements are quantized into 0.1 m segments called bins, where with proper thresholding the algorithm should be able to determine if a measurement in the histogram is from a lane marking or the road's surface . It was noted however that changes in surface roughness such as rumble strips and small obstacles on the side-strip of highways causes more scan points than actual painted lane markings which causes a "horizontal spreading" which can lead to detection errors when simply thresholding the histogram. In an attempt to mitigate the "horizontal spreading" effect, the gradient of the histogram is also analyzed. Once lane markings are detected, the vehicles lateral offset in the lane and yaw within the lane is determined. A truth measurement for accuracy could not be established, therefore a chart of detection rates was given. These rates varied from 16 to 100%, with an average detection rate of 87% for the lanes bounding the vehicle. A more advance approach is also give in [23] which still employs the same histogram and histogram gradient feature extraction algorithm, but with the use of use a modified version of the lidar. The modification added to their lidar is the addition of two mirrors on either side of the lidar which reflect the lidar pulses that would normally be reserved for scanning behind the lidar, towards the road, thus increasing the effective scan density. The lidar's ROI was also changed to scan approximately ±3 m in the lateral direction and 4 to 5.5 m in-front of the vehicle in an effort to reduce algorithm errors. A quality measurement acts as an additional bound which is based on the number of scan points from the various layers. A Kalman filter is employed in an effort to track the lane markings. With this algorithm, the researchers claim to detect solid lane markings about 95% of the time while only detecting dashed lane markings 35% of the time.

The histogram feature detection approach with the modified lidar presented in [23] is also employed in [13]. In [13] a ROI is defined at a distance of 0 to 30 m in-front of the vehicle and ±12 m in the lateral direction. As in [23], [13] was unable to calculate a truth position of their position in the lane, however they were capable of obtaining a truth measurement for the lane width in which they traveled, with a high degree of accuracy [13]. Additionally, they attempted to drive perfectly straight for small sections of road and determine if their algorithm reported any changes in position as an estimate of the accuracy of their system, which they did with an average accuracy of 0.25 m [13].

A similar histogramming technique to [23] and [13] was employed in [24] with the use of a 6 layer DENSO automotive lidar scanning between 10m and 25m in front of the vehicle. However, in [24], a histogram like structure is created using polar coordinates instead of Cartesian coordinates. This quantized polar coordinate histogram is known as a lane detector grid. This grid is not compensated for ego-vehicle motion, and each bin is created by simply choosing the value of highest reflectivity of the lidar measurements it will encompass [24]. It is noted however that averaging all measurements assigned to a bin is an equally valid method of quantization [24]. The theory behind the lane detector grid is that because all points in a row are equidistant from the origin, quick comparisons of reflectivity can be made without compensating for the large difference in distance of the various scan layers from the vehicle. Once the grid is constructed, lane markings are extracted using thresholding [24]. However, in order to calculate the vehicle's position in the lane, the lane detector grid is not used directly. The raw lidar scan is used to determine lateral position using the lane detector grid's result as a guide for selecting the lane marking from the raw lidar data to base the vehicle's lateral position on, which was tracked with the aid of an unscented Kalman filter (UKF). Not using the quantized data allowed for a more precise position result. Despite no truth data being available, [24] presents several graphs demonstrating the consistency of the algorithm to determine lane width as well as several plots of the lidar's data laid over an image. It is noted that this algorithm works best on roads with dark asphalt with highly contrasting lane markings raised approximately 2mm above the road's surface, typical to those lane markings found in Germany. The worst road surface for this algorithm is concrete. It was additionally noted that the combination of heavy rain and poor drainage on the roadway significantly influenced the ability to consistently detect lane markings in adverse weather. Finally it was noted that dazzling occasionally occurred at sunrise and sunset, however it was found that the lidar was not as influenced by bright light as were accompanying camera sensors [24].

A Velodyne HDL-64E lidar is used in [22] which scanned at a rate of 10 Hz with 64 layers and a resolution of 0.09° horizontally, mounted on the roof of the vehicle allowing a 360° field of view. Several lidar scans are taken and mapped into an ego-centric coordinate frame with the use of a fused GPS/INS system. After non-road surface features are removed an additional filter is applied to the reflectivity data so that only points with an absolute reflectivity intensity larger than the median intensity of each scan is taken into account. Once this initial filtering is complete the lidar data is mapped into a feature grid, which effectively acts as a way of quantizing the lidar data cells. Once complete, lanes are detected using a Radon transform, where the lane markings are found by locating their corresponding maxima in the Radon plane. No truth data was provided, however it was noted that the proposed algorithm was able to detect lane markings in the presence of shadowing, direct sunlight, and at night. A similar technique is applied in [26] with a DENSO lidar which is capable of scanning at 10Hz with 6 layers at a resolution of 0.08°, however, instead of a Radon transform a Hough transform was employed. Additionally, [26] created a histogram of the distance from the extracted lane markings to the lane's center line. This was used in an attempt to mitigate disturbances due to erroneous lane markings as well as narrow the search area of potential lane markings. The algorithm's success was established by overlaying the predicted lane widths over an image taken of the lane markings.

A lane tracking algorithm was also presented in [2] for lane detection in urban environments, in which two six layer laser scanners are used with a horizontal angular resolution of 0.1° and an angle of 1.57° between layers which search for lane markings between 5m and 30m in front of the vehicle. However, only layers one through five where used for lane detection, the sixth layer was reserved for obstacle detection. Each lidar was used to detect a single lane marking on either the left or the right side of the vehicle causing a gap in front of the vehicle where it was assumed no lane markings would exist without first passing one of the laser scanners. The lane detection algorithm first pre-filters the data, by removing measurements that were likely to be obstructed by an object as determined using layer six of the lidar scanners and an object tracking algorithm. While the specifics of the lane extraction algorithm are withheld it is noted and an extended Kalman filter (EKF) is used to track the distance of the vehicle to the right lane, the lane's width, and the yaw of the vehicle within the lane [2]. An additional data association algorithm is used in an effort to exclude possible false detections by using data about known surrounding objects, however, it is noted in [2] that this approach does not prevent all forms of false detection. A ground truth could not be established in [2], however the algorithm's performance was compared to an accompanying camera system running a similar EKF algorithm. The lidar based algorithm estimated lane width to within 0.09m to 0.05m to the lane width of that measured by the camera. Vehicle position in the lane differed only on the range of 0.02m to 0.01m between the lidar and camera systems [2].

2.4 Calibration and Attitude Determination background

It is necessary for many applications, including vehicle safety to be able to relate a sensor's measurements to the vehicle's coordinate frame, be it local position of the vehicle or distance and angle to an obstacle or point of interest. For this to be accomplished the sensor's reference frame must be known relative to the vehicle's reference frame, thus sensor measurements can be related in a meaningful way to the vehicle. It is common for sensors such as lidar systems to not be mounted with perfect alignment to the vehicle's coordinate frame, therefore it is necessary to be capable of determining how the lidar's coordinate frame relates to the vehicle's coordinate frame which is determined through a process known as calibration [5]. Lidar calibration can vary greatly in complexity and technique, but to be able to fully relate the sensor's coordinate frame to the vehicle's, the pitch, roll, and yaw of the lidar relative to the vehicle must be determined. It is possible to make assumptions to ease the process of lidar calibration, such as the only error is pitch, or that there is negligible yaw offset as done in [37]. Calibration techniques are often complex, highly non-linear, and often require the use of either known landmarks, known excitation, or the scanning of a known surface such as in [4, 38, 12, 28]. However, it is often infeasible to assume that well known landmarks will be present or perfectly controlled excitations such as a known change in position or roll can occur, especially for the casual user or for field calibration.

A calibration technique is presented in [5] for the calibration of a 2D lidar. This algorithm attempts to determine its pitch, roll, and yaw in reference to a specially created pyramidal landmark by exploiting known geometric relationships of the landmark, specifically those involving conic cross sections and ray parametrization of polypods [5]. The algorithm attempts to minimize an algebraic error metric and an iterative refinement scheme to solve the equations in close form based on euclidean rotations that define the attitude of the lidar in relationship to a landmark [5]. An accuracy of one degree of attitude error is reported despite their truth solution only claiming an accuracy of two degrees [5]. It is worthwhile to note that this attitude accuracy measurement is not listed as individual errors in roll, pitch or yaw, but as a single measurement, for which no other details are given.

Formulations for determining a 3-D lidar's attitude to a reference plane with reference points is given in [12]. The presented equations allow the user to determine the pitch and roll of the lidar to the reference plane by the introduction of points on the reference plane whose positions are known. Results for the accuracy of the measurements however were not presented in [12].

A calibration technique is presented in [38] in which a 1-D lidar in the visible spectrum is used in conjunction with a robotic arm and a video camera for feedback. The ability to successfully calibrate the laser to the robotic arm's reference frame is demonstrated by the use of moving the robot's end-effector so that the laser moves to six unique positions; the actual location the laser is contacting is recorded by a stationary camera. By comparing the robotic arm's motion to change in the laser's position, the laser's attitude to the robotic arm can be determined through the simple use of least squares [38]. A similar technique is presented in [28] where a robotic arm is used in conjunction with four 1-D lidars. The robotic arm is then put through a series of known maneuvers, and the plane defined by the lidars measurements are analyzed to determine the attitude of the lidar system to within sub degree accuracy according to the simulations run in [28].

It is worth noting, that many calibration techniques can be applied for use in attitude determination. Attitude determination is the process of calculating the vehicle's attitude, pitch, roll, and yaw, in reference to an environment or global coordinate frame, as opposed to a vehicle's coordinate frame. Attitude determination techniques based on lidar typically assume an already aligned lidar system such as in [37]. Where beacons, known as corner cubes are used, which are placed at known locations. An attempt to mimic a single multi-layer lidar system is accomplished by using two single layer lidars mounted at different known elevation angles. There are several initial assumptions made which include that the lidars are placed at the origin of the vehicle's coordinate frame, that the lidar's coordinate frame is aligned to the vehicles coordinate frame, and that the vehicle initially it not pitching or rolling. It is also shown that the algorithm introduced has the ability to then determine the vehicles pitch and roll assuming both lidars are contacting the same corner cube beacon. Naturally the vehicles location and yaw in reference to the beacons can also be determined. The method proposed is validated through simulation assuming the only error source is in the angular measurement reported by the lidar of one mrad or 0.0573deg. Several plots of the simulated method are shown and [37] simply states that the attitude is measured with enough accuracy for their desired application.

A novel attitude determination technique is presented in [4] where a 3-D AccuRange 400 lidar is used to aid an unmanned rotocraft in landing or taking off of a ship at sea whose deck is assumed to be undergoing dynamics. The lidar used in [4] produces a circular beam as opposed to a horizontal sweep, onto the ship's deck. The geometry of the circle is then analyzed and the pitch and roll of the rotocraft relative to the deck can be determined. Real-time truth data was not able to be obtained in [4], however simulated results predicted errors of less than 1.5°. A similar concept is employed in [27] where an object of known geometry is used to calibrate the lidar to a reference plane defined by an aircraft.

2.5 Roll Estimation Background

There are two types of rollover, tripped and un-tripped [31, 30]. Tripped rollover is typically characterized by the vehicle interacting with the environment in an unpredictable way, such as the vehicle impacting curb or guard rail, or one side of a sliding vehicle's tires digging in due to soft soil [31, 30]. However, driver induced un-tripped rollover typically occurs during more normal driving scenarios, and can come about due to severe vehicle maneuvers such as obstacle avoidance or cornering speed [31, 30]. Focus is placed on estimating vehicle roll in this thesis.

The ability to detect attitude is useful in many navigation and safety systems, however this is especially true in rollover scenarios, where typically the roll of the vehicle relative to the road is not known and must be estimated [17]. This relative roll measurement must often be estimated through the use of lateral and vertical accelerometers as well as roll rate sensors as seen in [17, 33, 34, 8] or through measurement of suspension deflection such as in [17]. This ability to detect or estimate relative roll is useful because most rollover methods rely on inertial measurements which can detect only a global roll or global roll rate and not the angle or angular rate with respect to the road, and therefore cannot directly differentiate between a banked road with no vehicle roll, and a level road with vehicle roll [17].

A method for estimating both the roll angle and roll rate of the vehicle relative to the road's surface using lateral accelerometers which sense the lateral acceleration of a vehicle in a turn, and roll rate sensors is proposed in [17]. The issue of banked road's is dealt with by assuming that changes in roll rate are small due to road bank, thus the change in bank angle is estimated by taking the measured roll rate, and differencing it from the estimated roll rate estimated by the lateral accelerometers, and low-pass filtering the result. It is noted that the method of rollover detection presented works well on level roads while the vehicle undergoes sharp maneuvers but is sensitive to a change in road bank angle, and often underestimates slowly varying roll angles. To combat these errors, the authors introduces a second technique based on measuring suspension deflection. The idea being that a sensor is located at each wheel to measure suspension deflection, to give a relative position of the wheel with respect to the vehicle's body. This method tracks the roll angle with respect to the road well, however suffered from underestimation for large roll angles as noted in [17]. While it is noted that there are many techniques devised to detect rollover this information is simply given to show that the ability to determine vehicle roll angle with respect to the road is desirable and can be difficult to measure directly.

2.6 Non-Linear Error Propagation

As previously mentioned in Section 2.4 the process of lidar calibration and attitude determination can be highly nonlinear. This is often due to the functions used to transfer coordinate frames such as converting from polar to Cartesian coordinates as well as representing rotations such as pitch, roll, or yaw which are highly non-linear. These non-linearities often make it difficult to determine how errors in measurements can propagate. This problem is often inherent when using a lidar because the lidar often reports measurements in polar coordinates which need to be transformed into Cartesian coordinates, for most navigation algorithms. While there are several techniques for determining how errors propagate through nonlinear systems, the most popular method is by local linearization, such as in the case of an extended Kalman Filter (EKF) [1]. Despite its popularity, the EKF has been shown to potentially yield extremely inaccurate estimates of statistics [1]. In an effort to obtain accurate estimates of noise statistics, an Unscented Transformation (UT) is used in this thesis. The UT is based on the principle that "it is easier to approximate a probability distribution than it is to approximate an arbitrary non-linear function or transformation" [1]. Hence the UT works by constructing a set of "sigma points" which are deterministically selected to have known statics, such as the first, second or high order moments, of a given measurement [20]. The non-linear transformation is then applied to the sigma points. By analyzing the statistics of the transformed sigma points the unscented estimate can be obtained [20]. The UT in this thesis was used to estimate the errors in each attitude measurement in an effort to minimize the affects of noise on measurements in these highly non-linear equations.

2.7 Thesis Outline

In Chapter 3 an algorithm for detecting lane markings using a multi-layer lidar is presented. Validation and truth data will provided to show overall functionality of the algorithm. Validation of the lane detection algorithm will take the form of both a comparison of the estimated position of the vehicle using the lidar to a truth solution of the vehicle's position in the lane obtained via DGPS and precision map, as well techniques similar to those mentioned in 2.3 where a DGPS truth solution was unavailable. In Chapter 4 a technique for both calibrating a lidar to a vehicle's axes is presented as well as an algorithm for determining the vehicle's pitch and roll. Chapter 5 will include test and validation data for the calibration and attitude algorithms that will take the form of both controlled laboratory testing as well as vehicular testing. Finally concluding remarks and future work are made in Chapter 6.

2.8 Contributions

This thesis contributes to the research field specifically by developing a novel lane extraction method for vehicle safety systems, which is capable of adapting to changes in road types, widths, paints, and varying mounting locations in real-time. Additionally, results are provided of the above method using DGPS as a validation technique which allows for empirical validation of the algorithm. Additionally, results are provided as a comparison to other methods currently employed by preforming such tests as lane width estimation and position estimation for similarly length ed experiments [3, 11]. Finally, this thesis introduces a novel lidar calibration and attitude determination algorithm for vehicle safety systems. This algorithm is capable of auto-calibrating itself to the vehicle's axes as well as determining the vehicle's pitch and roll provided the vehicle is on a planar surface [9, 10]. This technique is shown to be capable of determining the vehicle's attitude to sub-degree accuracy when compared to a commercial GPS based attitude system.

In short, the following are contributions that this thesis makes to the research field:

- Development of a novel lane extraction method for vehicle safety systems [3, 11].
- Presentation of DGPS results in comparison to lane extraction method as a verification technique[11].
- Development of three-dimensional lidar calibration and vehicle attitude estimation algorithm, which requires only a planar surface for calibration [9, 10].

Chapter 3

Lane detection and tracking using multilayer lidar

This chapter presents a lane detection algorithm that uses a multi-layer lidar to extract lane markings from a road's surface based on the difference in reflectivity between the lane markings and the road's surface. This extraction algorithm is shown to run in real-time at 10-Hz. The Algorithm will begin by first calibrating itself for the height above the road as well as for it's mounting pitch. The algorithm will then create a narrowed search array from which to extract the lane markings. The lane markings will then be extracted based on a minimum arrow to a nominal lane model. Once the lane markings are detected they are tracked for added robustness. This algorithm is shown to be capable of dynamically accounting for not only its mounting, but changes in road width, surface reflectivity, as well as paint color. Finally this algorithm is shown to be capable of mitigating errors as well as detecting and extracting a lane markings with a high degree of accuracy and consistency

3.1 Hardware

The sensor used in this thesis for lane marker detection and position estimation is an Ibeo ALASCA XT. The ALASCA XT is an automotive grade three dimensional, time-of-flight lidar. Thus, as opposed to more typical two dimensional lidars which have a single horizontal beam, the ALASCA XT has four vertically diverging beams known as layers.

The individual layers are generated from a single static photo diode that generates the laser, and a rotating mirror to angle and direct the beam. Despite having only one transmitter (the laser), the Ibeo has four receivers to detect the returning lidar's pulse [18]. Each layer is denoted with capital letters A, B, C, and D, each having a maximal vertical divergence of 1.6°, 0.8°, -0.8°, and -1.6°. One sweep of these multiple layers constitutes a

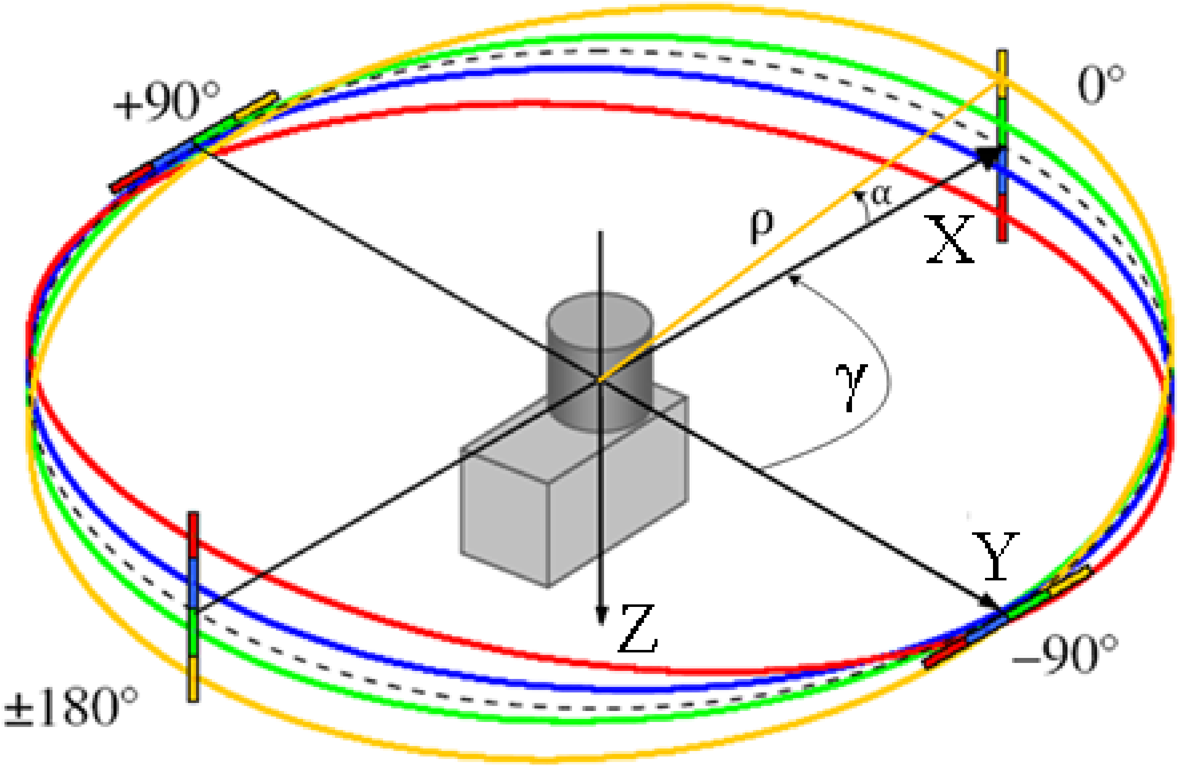

Figure 3.1: Representation of lidar scan and coordinate frame

scan. As shown in Figure 3.1 the vertically diverging layers are neither lines at a fixed vertical divergence nor are they perfect sinusoids, but are rather shortened cycloids [18]. The lidar reports measurements in polar coordinates where ρ is the distance to the object, γ is the horizontal angle of the distance measurement, and α is the vertical angle of the distance measurement as shown in Figure 3.1.

Additionally, the ALASCA XT's scan resolution is both a function of scan rate as well as scan angle as shown in Table 3.1. Thus it is important to note that the scan is more dense nearer the X-axis which is the forward looking direction for the lidar. Varying scan density is often useful in automotive applications because it allows a dense scan directly in front of the lidar which is often the area of most interest, and tapers off accordingly to the sides, which are typically areas of less relevance [18]. Additionally, unlike many other lidar systems the ALASCA's scan angles are not rigidly set, meaning that it doesn't measure $\gamma = 45°$ every scan; instead it might report a measurement at $\gamma = 45.1°$ or $\gamma = 39.9°$ and so on.

Table 3.1: Lidar resolution compared to scan rate and scan angle

	Resolution	
Angle	12.5Hz	25Hz
0° - 16°	0.25°	0.5°
16° - 60°	0.5°	1°
60° - 120°	1°	2°
120° - 164°	2°	4°

In addition to reporting distance and angle measurements, the lidar is capable of reporting a measurement of reflectivity, a measurement known as echo width. This measurement allows for the algorithm to discern the lane markings from the road's surface. With each measurement pulse of the lidar, the lidar is capable of detecting multiple reflections of the returning beam. This means that if there is a rain drop between the lidar's pulse and the road surface, the lidar will detect both the reflected beam of the light from the rain drop as well as the reflection of the beam from the road's surface due to any part of the beam not obstructed by the rain drop or that went through the rain drop. For each reflection of the beam, a corresponding distance and reflectivity value is measured. Up to four reflections per measurement are capable of being detected. This multi-reflection ability of the lidar allows for the potential to develop robust algorithms that are less sensitive to environmental conditions.

3.2 Nomenclature

In order to facilitate effective communication of the equations used in this section, the following standards are employed. As stated in section 3.1, the different lidar layers are denoted as A, B, C, and D, corresponding to 1.6°, 0.8°, -0.8°, and -1.6° of maximum vertical divergence. If an equation does not specify a specific layer, it is assumed that the equation involves only one layer, and is invariant of which layer. If an equation involves two arbitrary layers, these will be denoted as X and Y. Indices i, j, and k will denote an arbitrary index of a lidar measurement and will be denote via subscript. Hence A_{ρ_i} would denoted a specific range measurement of layer A. If an equation assumes the data is only taken at a specific horizontal angle, that angle will be specified and all indices will correspond to where this angle occurs. Hence equation $\rho_i cos(\alpha_i)$, $\gamma = 0$ corresponds to the range measurement where $\gamma = 0$ multiplied by the cosine of the vertical divergence where $\gamma = 0$. If a value is calculated using two different layers, this will be denoted with the layers as sub-scripts, hence $arbitraryValue_{A,B}$. The resolution of a measurement will be represented using the Δ operator, hence Δ_γ would indicate the lidar's angular resolution. The lane width is measured from the center of the lane markings will be denote as LW, and the width of the vehicle as measured by the distance between two tires on the same axle taken from the outside face of the tire, will be denoted as VW.

3.3 Mounting

The lidar is mounted approximately 1.5m off the ground atop a roof-rack attached to a Hyundai Sonata. It is assumed that the lidar is mounted to align with the center-line of the vehicle. The lidar is pitched at approx -22° so that all of the lidar's layers are contacting the road's surface directly in front of the lidar. The lidar is therefore measuring approx 2m in front of the vehicle. While this does not provide an ideal mounting location for obstacle avoidance where the lidar would need to be much further forward looking, it is ideal for lane detection given the varying resolution of the lidar with the scan angle, because this mounting allows for greater resolution at the lane markings. To illustrate this the current mount is compared to a more typical mounting location, such as on the front bumper where the lidar is looking straight down in an attempt to mitigate affects from automobile motion and capture only road data. Additionally the mounting location was compared to those in [13, 23, 24]. The data in Table 3.2 shows the resolution on the road's surface for a vehicle centered in its lane measuring to the lane marker defining its lane as well as the resolution of the adjacent lane's furthest lane marking. It is worth noting that because the lidar is forward looking, it can potentially scan the vehicle in front of the of the lidar. Despite this being

Table 3.2: Mounting location comparison

Mounting:	Roof	Bumper	[23]	[24]	[13]
Height	1.5m	0.5m	0.5m	0.5m	0.5m
Pitch	-22°	-90°	-5.7°	-1.9°	-1°
Forward Dist	1.7m	0m	5m	15m	30m
Lane marker resolution	1.6in	4.6in	1.7in	2.6in	5.2in
Adjacent lane marker resolution	4in	35in	4in	2.9in	5.3in

possible, it has been shown unlikely in practice due to the fact that safe driving typically dictates greater than a 2m gap between vehicles, however this is occasionally encountered at traffic moving at speeds less than five miles per hour such as near a stop light or perhaps in heavy congestion. However this potential of mis-detection is considered acceptable due to the low probability of a lane departure occurring at these speeds. The assumption that a 2m gap between vehicles is maintained, allows for the elimination of an additional algorithm to remove erroneous obstacles such as other vehicles from the scan data allowing for increased processing speed. Additionally, because reflectivity is a function of both distance and the surface composition of the object, maintaining a relatively close distance between layers can allow for easy comparison of layers if needed. Finally the yaw of the vehicle in the lane can potentially cause measurement errors at this distance, meaning that if the vehicle were in a sharp turn the lidar might predict a larger lane width than the true value. If yaw in the lane needed to be predicted, having the measurements close to the vehicle would prove difficult because of the minimal spacing between layers. Conversely, yaw in the lane should be less of an issue for a lidar that is scanning directly in front of the vehicle such as the mounting location used in this research, than one scanning at greater forward distances.

3.4 Calibration

It is important for lane detection applications to know the expected resolution of a scan in order to ensure lane marker detection, as well as how far forward a scan point may be contacting the road to know if obstacle removal or yaw prediction is necessary or feasible.

To do this, the algorithm first calibrates the lidar's pitch making the assumptions that the vehicle is on a planar surface and that there is neither a roll offset nor yaw offset as seen in Equation 3.1.

$$\theta_{X,Y} = -Y_{\alpha_j} + \arctan((X_{\rho_i}\cos(X_{\alpha_i} - Y_{\alpha_j}) - Y_{\rho_j})/X_{\rho_i}/\sin(X_{\alpha_i} - Y_{\alpha_j})) - 90° \, \gamma_{i,j} = 0° \quad (3.1)$$

Where θ as seen in Figure 3.2, is the pitch calculated by using layers X and Y, and is measured relative to the vehicle's x-axis . It is assumed that all ρ values are taken at $\gamma = 0°$. This not only simplifies the math, but also allows for maximum vertical separation between scans, which should aid to minimize any errors due to noisy data. Typically, one-hundred scans are taken and the values of the measurements are averaged in a further attempt to mitigate any error due to noisy data. A total of six pitch values can be determined if every combination of layers is used. The average of the six computed pitch angles is found as shown in Equation(3.2) in order to obtain the final pitch measurement. A typical pitch for the lidar when mounted on the roof of the Sonata is approximately -22°.

$$\theta = (\theta_{A,B} + \theta_{A,C} + \theta_{A,D} + \theta_{B,C} + \theta_{B,D} + \theta_{C,D})/6 \quad (3.2)$$

Once this average pitch measurement is obtained the height of the lidar can be calculated as shown in Equation(3.3) where the ρ measurement is still taken at $\gamma = 0°$.

$$h_X = \rho_k \cos(\theta + \alpha_k), \, \gamma_k = 0° \quad (3.3)$$

The same one-hundred averaged measurements used in the computation of the pitch are used again here. Typical height values for the Sonata are approximately 1.5m as measured along the vehicle's z-axis as shown in Figure 3.2. Using the above formula, four different heights can be calculated, the average of which shown in Equation(3.4) is taken to be the

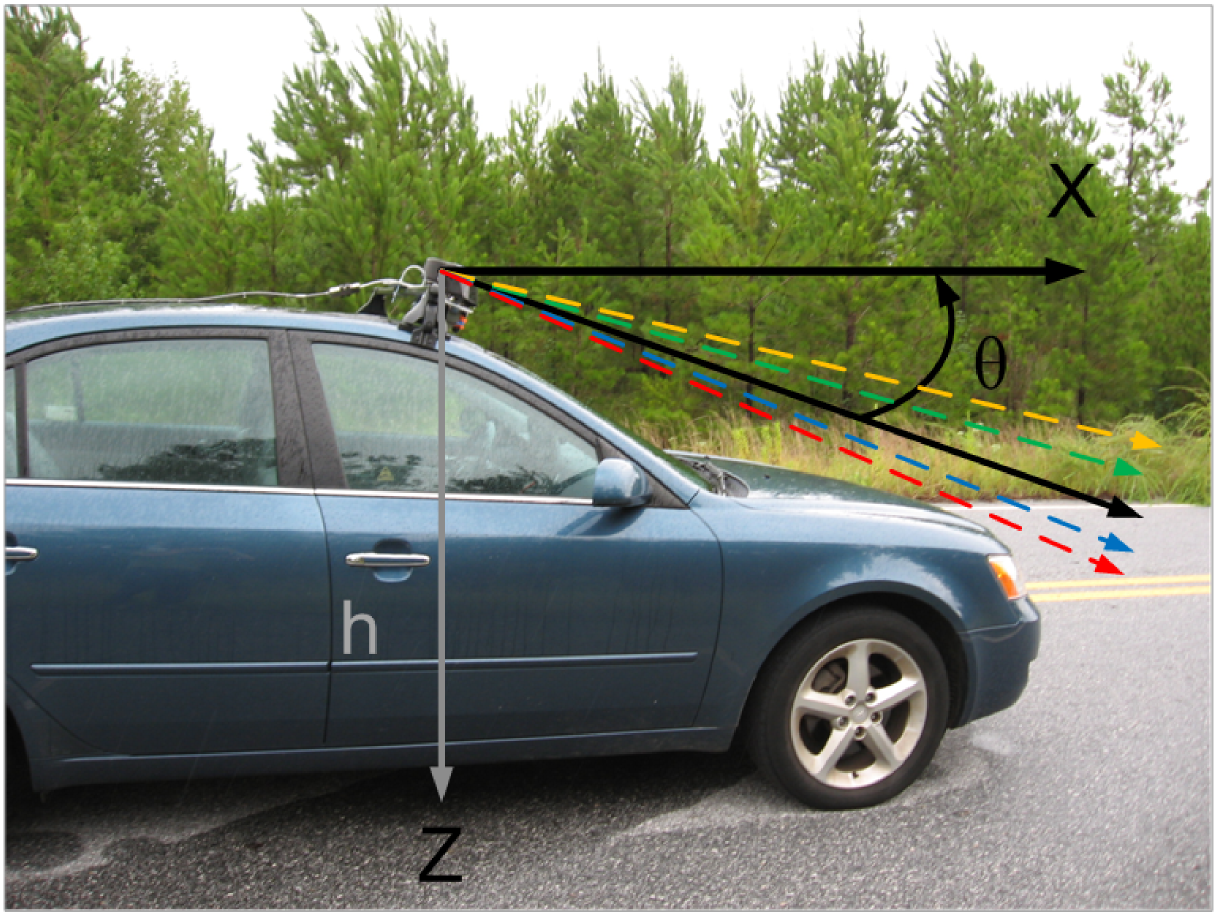

Figure 3.2: Determination of lidar height and pitch

correct height which will be used for both measurement resolution calculations as well as the determination of the forward looking distance.

$$h = (h_A + h_B + h_C + h_D)/4 \tag{3.4}$$

This height value is only calculated at initialization and is assumed to stay constant throughout the test. With the height and pitch of the lidar found, an estimate of the measurement resolution at the lane markings can now be determined as shown in Equation(3.5), as well as the scan distance in front of the vehicle as shown in Equation(3.6). The measurement resolution will allow the algorithm to determine whether lane markings of a given lane width are detectable by comparing this measurement to the standard lane marker width.

This information will also prove valuable later when scanning boundaries need to be established.

$$\Delta d_{y-axis} = \left| LW - \frac{VW}{2} - \tan\left(\arctan\left(\frac{LW - \frac{VW}{2}}{\frac{h}{\sin(-\theta-\alpha)}} \right) + \Delta_{\gamma} \right) \right| \tag{3.5}$$

$$d_{x-axis} = \frac{h}{\tan(-\theta - \alpha)} \tag{3.6}$$

3.5 Detection

Detection of the the lane markings utilizes the principle that the lane markings on the roadway are more reflective than the road's surface as seen in [23, 13, 24, 22, 26, 11]. Therefore the lidar will scan the roads surface and receive both distance measurements between the lidar and the road's surface as well as a measurement of the reflectivity of the road's surface at the location of that distance measurement. The detection algorithm will bound the scan so that only the lane in question is being scanned. The algorithm will then detect the lane markings using using a combination of scan matching and minim root mean square error (RMSE). Once the lane marking has been detected, a narrowed search area is created for future detection. Finally the position of the vehicle in the lane is calculated and this final position is filtered and reported.

3.5.1 Bounding

In an effort to minimize computation, processing time, and false positives, bounding is employed which reduces the amount of road's surface that the lidar scans. The bounding area is established by finding the maximum horizontal angle at which the lidar will measure a lane marking regardless of position of the vehicle in the lane. This is done by assuming the lidar is mounted in the center of the vehicle and then subtracting half the wheel base width from the typical lane width. This distance is the horizontal distance which the lidar should be capable of detecting a lane marking in its lane, and represents the distance the lidar must be capable of detecting the left lane marker if the right wheels are contacting the right lane marker and vice-versa. The angle associated with this horizontal distance becomes a bound. Any horizontal angular measurement from the lidar is not process if it is outside this bound which is referred to simply as the scan bound. However despite this bound guaranteeing the lidar the ability to scan both lane markings provided the car is in the lane, it will also introduce erroneous data due to a portion of the bounds always being outside the lane. Often this erroneous data takes the form of rumble strips, grass, or even other vehicles which can introduce errors into the lane detection algorithm. This is illustrated in Figure 3.3 where the red lines radiating from the lidar represent the scan bounds that the lidar will search over, and the horizontal red line, representing the road's surface over which the lidar will attempt to detect lane markings. The angle at which to establish these angle bounds is presented in Equation(3.7).

$$Angle\,Bound = \arctan\left(\frac{LW - \frac{VW}{2}}{\rho_k}\right),\ \gamma_k = 0^\circ \tag{3.7}$$

If no lane width data is presently known about a lane, such as at initialization, then a nominal lane width of twelve feet is assumed. However, if an estimate of the lane's width is available from the algorithm, this updated lane width estimate is employed in determining the scan angle bounds. Hence, whenever a change in lane width is detected, this new lane width is used to establish new scan bounds provided that lane width estimate is no more than two iterations old, in which case the nominal lane width is assumed.

3.5.2 Scan Matching

In an effort to facilitate effective communication, it is important that the reader refer to Figure 3.4 and corresponding Figures 3.5 and 3.6. Figure 3.4 depicts a common roadway with a solid white lane marking to the right of the vehicle denoted by the number one, two solid yellow lines to the vehicle's immediate left denoted with numbers two and three, and

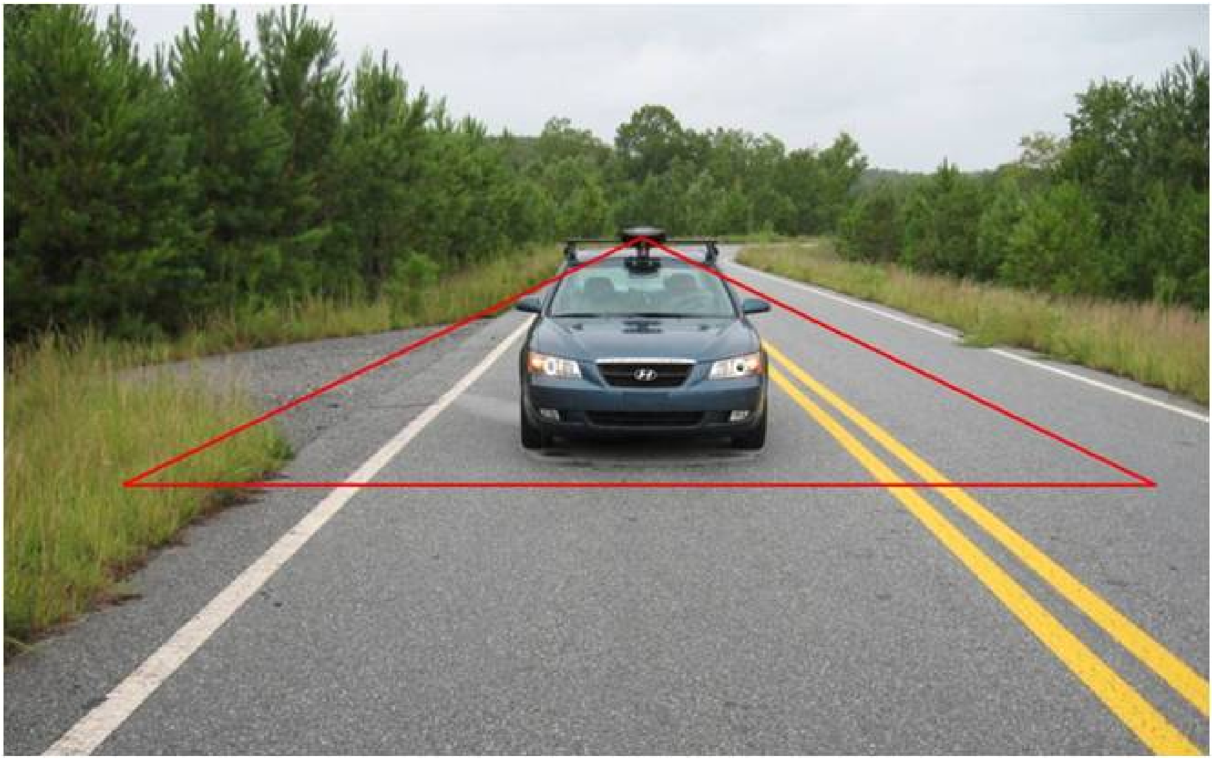

Figure 3.3: Scan Angle Bounds

another white lane markings bounding the adjacent lane denoted with the number four. Also note that the road is bordered by grass and there are two red lines running parallel to the road's edge. Figure 3.5 is a graph of 100 reflectivity scans averaged together representing a nominal lidar scan of the road shown in Figure 3.4 where the y-axis is echo width and the x-axis is the corresponding angle the echo width measurement was taken. Figure 3.5 also has two vertical red lines which should correspond to the road's edge. Finally, there are four spikes with numbers corresponding to those in Figure 3.4. Figure 3.6 is also a graph of echo width similar to that of Figure 3.5, however Figure 3.6 is merely a single noisy scan. Once again, Figure 3.6 has four numbered spikes corresponding to those in Figure 3.4.

The scan matching algorithm is the heart of the lane detection algorithm, the overall goal of which is to differentiate lane markings from the road's surface as well as other erroneous data. This is done through the use of matching each layer of the lidar's scan to an ideal scan and determining the RMSE error between them. While many lane detection algorithms are

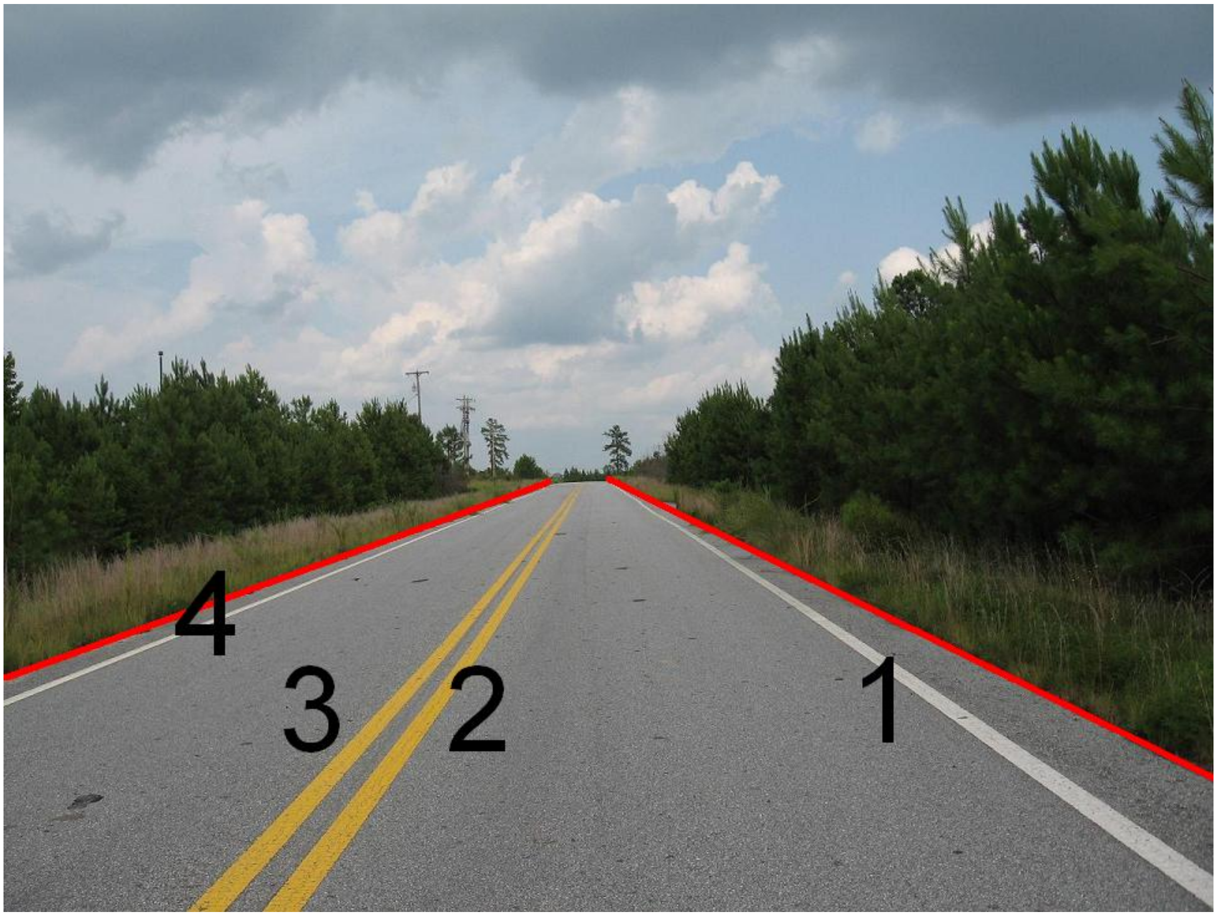

Figure 3.4: Typical Lane Markings

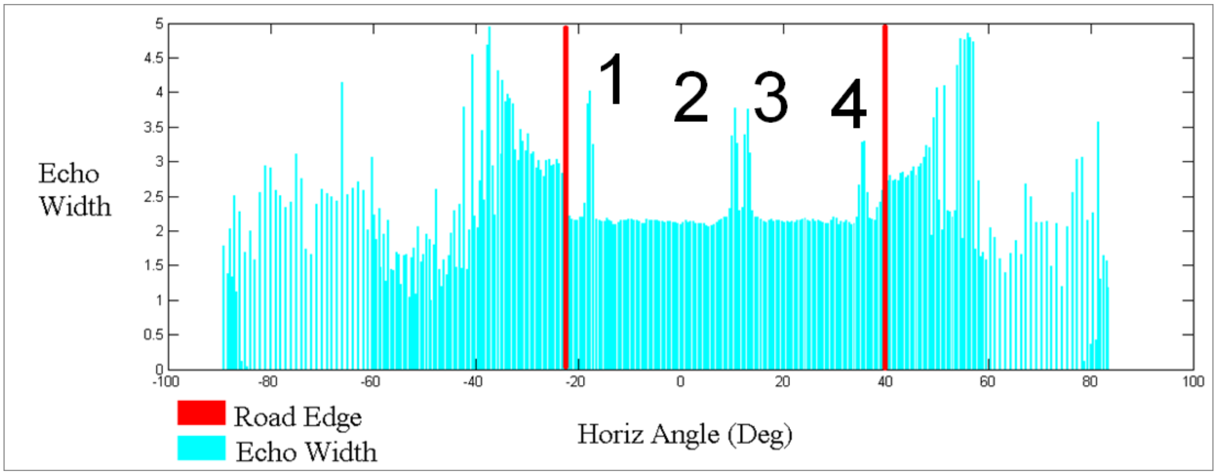

Figure 3.5: 100 Averaged Echo Width Measurements

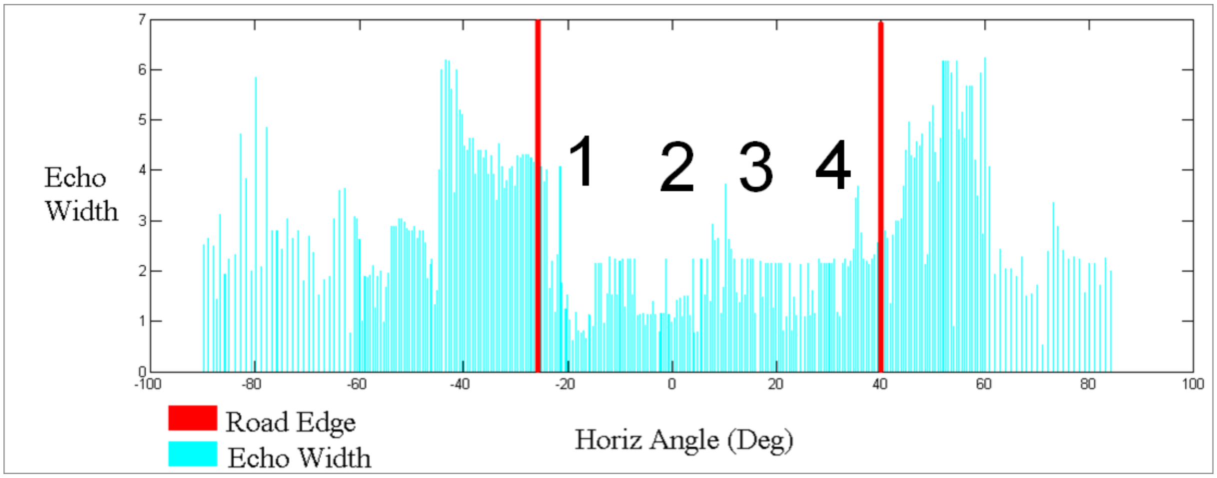

Figure 3.6: Single Noisy Echo Width Measurement

successful employing only bounding to distinguish potential lane markings from the road's surface and other erroneous data, it was noticed that determining a potential lane using only a detection threshold could prove error prone when the scan data was not ideal such as in Figure(3.6) where the sides of the road are significantly more reflective than the lane markings and would easily be mistaken for lane markings without more a sophisticated detection and discrimination algorithm than mere thresholding alone.

In order to preform scan matching an ideal scan must be created as shown in Figure 3.7. This ideal scan came from the fact that most lidar scans took on a form similar to those shown in Figure 3.5, where there is a flat, mostly constant portion of the scan representing the road's surface, typically, bounding either side of this constant portion are two spikes in reflectivity denoting the lane markings. From those spikes there can be either a further portion of constant data representing the road's surface being either the next lane or shoulder, and then finally a section of very noisy data often caused by grass, gravel, and other non-road data. Thus the ideal scan represents this constant level of reflectivity denoting the road's surface bounded by spikes denoting the lane markings. Hence the ideal scan is generated for each layer by scanning a portion of the road approx 0.6m wide directly in front of the vehicle and averaging its echo width data. This averaged value represents the constant value of the road's surface reflectivity. The lane markings are generated as being seventy-five percent

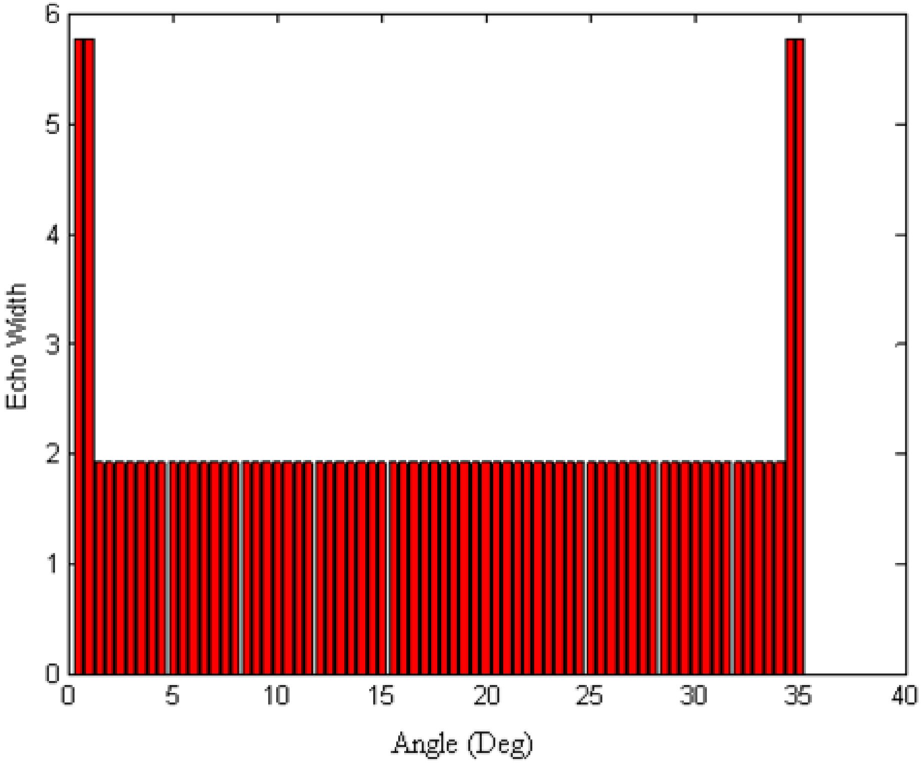

Figure 3.7: Ideal Scan

more reflective than the road's surface which was chosen empirically by comparing several different types of lane markings reflectivity to the road's surface. Because this ideal scan is constructed off of the lane's surface the ideal scan is able to easily transition road type and driving conditions making it very dynamic. Additionally the ideal scan takes into account not only the increase in reflectivity of the lane markings as many other lane detection algorithms, but also the relatively constant area of reflectivity represented by the road's surface.

Now that the ideal scan has been created it must be matched to the actual scan data. This is done first by establishing a minimum lane width and a maximum lane width, which will act as an additional constraint for the detection algorithm. Typically these values range from approximately 8ft to 14ft, which allow for more narrow arterial roads as well as wider suburban roads. The scan matching begins with a scan from one layer. That scans layer is divided into two subsections; the first being the section $\gamma_i = 0°$ to $\gamma_i =$scan bound left

(LB), and the second $\gamma_i = 0°$ to γ_i =scan bound right (RB) as established in Equation(3.7). The ideal scan begins with the left most portion of the actual scan overlapping γ_i =LB with the right most portion of the ideal scan being a distance of minimum lane width away. The RMSE between the overlapping ideal scan and the actual scan is taken. The right most portion of the ideal scan is then shifted along the actual scan one angle increment at a time until the distance over which the RMSE is calculated exceeds the maximum lane width. The ideal scans left most portion is then shifted one degree increment closer to $\gamma_i = 0°$. Again the right most portion of the ideal scan begins a distance of minimum lane width away and the process repeats. This processes of stretching and shifting the ideal scan continues until the left most portion of the ideal scan reaches $\gamma_i = 0°$, at which all possible lane width combinations and locations are exhausted for the search space. The minimum RMSE found for this process is considered to be the best estimation of the lane location. This process is repeated for each layer. Additionally this can be shown mathematically by allowing w_{min} to denote the minimum increase in k that is needed to view a lane of minimal lane width wide, and w_{max} as the maximum increase in k that is needed to view an area of maximal allowed lane width. Additionally the ideal scans left most index is denoted as γ_{ILS} and the ideals scans right most bound as γ_{IRS}, also, (γ_{LB}) will denote the location of the left scan bound and (γ_{RB}) will denote the location of the right scan bound . The number of indexes separating γ_{ILS} and γ_{IRS} is therefore not a fixed number and will increase and decrease throughout the scan matching process because they are merely intermediate indices to search with for a range of lane widths. Therefore the matching process would first begin with $\gamma_{LB} = \gamma_{ILS}$ and $\gamma_{LB+w_{min}} = \gamma_{IRS}$. The RMSE is taken between the ideal scan and the actual scan over the region defined by γ_{LB} and $\gamma_{LB+w_{min}}$. As stated above, the next step is to shift $\gamma_{IRS} = \gamma_{LB+w_{min}}$to $\gamma_{IRS} = \gamma_{LB+w_{min}+1}$ while keeping γ_{LB} the same and taking the RMSE error over the area overlapped by the ideal scan and actual scan until $\gamma_{LB+w_{max}} = \gamma_{IRS}$. Once this occurs, γ_{ILS} is reset to $\gamma_{LB+1} = \gamma_{ILS}$ and the process is repeated. This is presented in Equation(3.8).

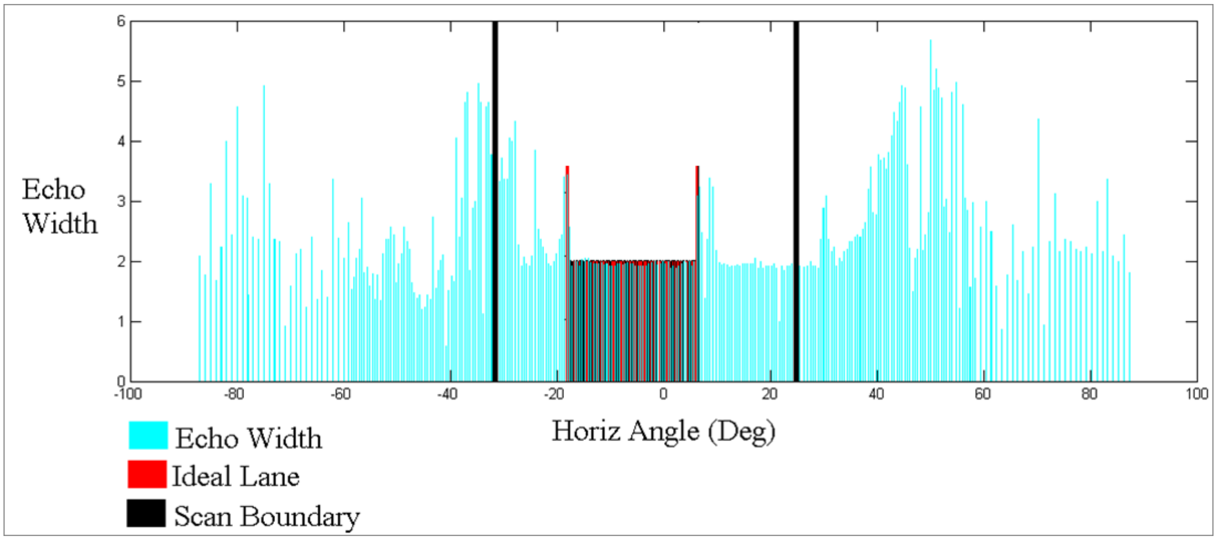

Figure 3.8: Ideal Scan and Echo Width Data

$$lane = min\left(\sum_{a=\gamma_{LB}}^{\gamma_a=0^\circ}\ \sum_{b=a+w_{min}}^{(a+w_{max})\leq\gamma_{RB}} \sqrt{\frac{\sum_{k=a}^{min(b,\gamma_{IRS})}\left(\gamma_{ILS+k}-\gamma_{LB+k}\right)^2}{b-a}}\right) \tag{3.8}$$

The ideal scan and the measured data will correspond to one another as shown in Figure 3.8 once the extraction algorithm is completed. It should be noted that this algorithm has an efficiency of $O\left(n^2\right)$and is therefore processor intensive. In an effort to obtain our real-time requirement of 10-Hz, the distance between points is not calculated at each iteration of k. Instead, a separation of angle between $\gamma's$ is used. Hence Equation(3.7) is utilized where the lane width is either the minimum lane width or the maximum lane width in an effort to establish a bound. While there is obviously the potential for slightly larger or narrower lanes to be found it should be remembered that the lane widths are simply a sanity check of the measurement and can be tweaked as need. Additionally, by merely doing a comparison of γ, data is processed significantly faster than determining the distance between two points with each shift or stretch of the ideal scan. Once the minimum RMSE has been established, the distance to the left and right lane markers is calculated.

Obviously, there will not always be two lane markings to detect. To determine which lane markings exist if either, the region of the scan overlapping the ideal lane markings is averaged. This average is then compared to the baseline established in the ideal scan. If the average echo width representing the lane spikes is less than a certain threshold (typically 30%) above the baseline, then the algorithm reports that no lane marking exists for the corresponding layer.

3.5.3 Windowing

In an effort to mitigate false positives, additional search bounds have been created for the scan matching algorithm. These additional bounds are known as windows. It is simply a way of further narrowing the search area in the scan matching algorithm which will in turn minimize processing time. This is accomplished by simply creating a narrowed search window around a scan, meaning that once a lane marking is successfully detected, successive scan matching algorithms place a bound of 4° around the location of where the lane marking was previously found as shown in Figure 3.9. The upper limit of this window is checked against the previously established bound of γ_{LB} or γ_{RB} and if a conflict occurs $\gamma_{i,LB}$ or $\gamma_{i,RB}$ is used. The minimum and maximum search window width is then checked to see if it is possible for the algorithm to attempt to choose lane markings smaller than the minimum lane width or larger than the maximum lane width. If this occurs the window closest to the vehicle is chosen to be the correct window to use and the other window is not used. The window closest to the vehicle is chosen as correct in the case of a conflict due it most likely being the one of most interest to a driver for vehicle safety.

Once a window has been established, the window is used until no lane marker is found in this window some threshold number of times, typically two in this thesis. This allows for dashed lane markings to be easily tracked because it allows the lane to leave the window and be reacquired while still having a minimized search area. A final check is also preformed on whether to continue using the narrowed search window, which compares the last result from a particular layer to the final solution of the previous iteration. The theory behind this test is that if one particular layer is straying greatly from the average or there are large

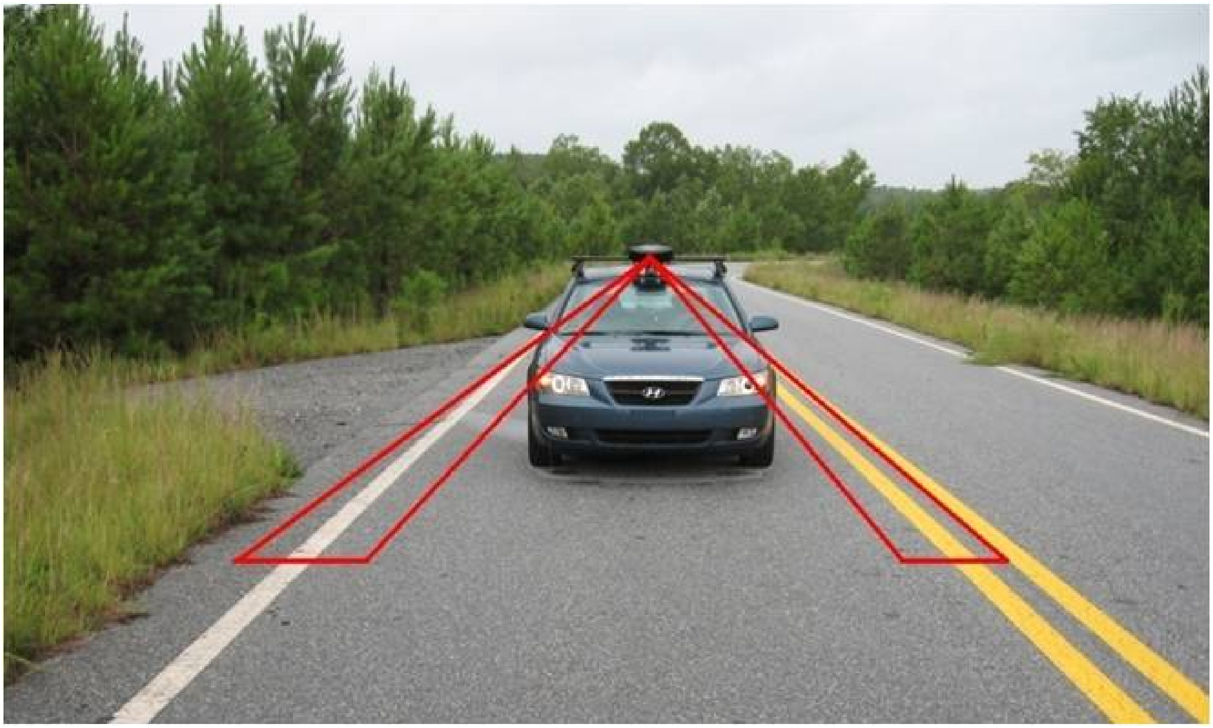

Figure 3.9: Scan Windows

inconsistencies between layers than this check will mitigate these errors. If the previous result for a particular layer and the final position solution of the previous iteration differ more than 0.52m the window bounds are once again reset.

3.5.4 Filtering

After all four layers have been searched for lane markings, and the individual distances to the left and right lane markings are found, a weighted average of these distances is computed. The weights are generated by finding the variance of the last 10 results from a particular layer. Layers with a lower variance are weighted higher in an effort to give preference to a layer that is detecting lane markings more consistently. The filtered results of the left and right hand lane measurements are denoted as d_{Ll} and d_{Rl}. When both lane markings are found, the total lane width $(d_{Rl} - d_{Ll})$ is determined and saved. When only one lane marking is found the known distance to one lane marking is used to calculate the distance to the lane marker that was not located, which assumes the lane width has remained constant. The distance from the center of the lane is then determined. Position in the lane is calculated as the distance from the center of the lane (d_{FC}), where the coordinate frame of the lane is also in the NED frame, with $y = 0$ being at the center of the lane. If both lane markings exist, it is a simple matter of subtracting the horizontal distance between the center of the scan to the right lane (d_{Rl}) which will be a positive number from the distance from the center of the scan to the left lane (d_{Ll}) which will be a negative number. Taking the average of these measurements and changing the sign to that the result agrees with our coordinate system as seen in equation 3.9 will give the position of the vehicle in the lane.

$$d_{FC} = \frac{-(d_{Ll} + d_{Rl})}{2} \tag{3.9}$$

If only the left or right lane marking is found, the position in the lane if found using Equation 3.10 or Equation 3.11, where the lane width from a previous measurement where both lane markings where found is used.

$$d_{FC} = \frac{LW + d_{Ll}}{2} \tag{3.10}$$

$$d_{FC} = \frac{LW - d_{Rl}}{2} \tag{3.11}$$

If no lane markings are found the algorithm simply does not report a distance, instead it sets a flag to indicate this has occurred. Once the position in the lane has been calculated the result is filtered before it is reported. This filtering is simply an attempt to filter out any jumps or spikes in position that might have occurred due to erroneous data. The filter used is a single state Kalman filter as seen in Equations (3.12-3.16) in which its only state is distance from the center of the lane.

$$\hat{x}_k^- = \hat{x}_{k-1} \tag{3.12}$$

$$P_k^- = P_{k-1} + Q \tag{3.13}$$

$$K_k = P_k^- \left(P_k^- + R\right)^{-1} \tag{3.14}$$

$$\hat{x}_k = \hat{x}_k^- + K_k(z_k - \hat{x}_k^-) \tag{3.15}$$

$$P_k = (1 - K_k)\, P_k^- \tag{3.16}$$

3.6 Test Procedure

To confirm the functionality of the algorithm, truth data was gathered by surveying the National Center for Asphalt Technology's (NCAT) 1.7 mile closed track located in Opelika, Alabama. With the aid of differential GPS, each lane marking was surveyed for the entirety of the track. The survey consisted of taking two measurements, one being the center of the left lane markings and the other being the center of the right lane markings. Those two measurements where averaged in an effort to determine the center of the lane where the vehicle's position would be based. For these tests the lane markings to the right of the vehicle are solid white, and those to the left are striped white. Despite being a closed track, it provides a very realistic representation of actual driving conditions due to it having multiple types of asphalt, having sections where no lane markings exist, rumble strips and typical highway wear due to other testing that takes place there.

In an effort to test the lidar's ability to detect lane markings for multiple road types and driving scenarios, it was necessary to also collect data at other locations. For non-track results, the truth metric used in [23] for detection rates will be given as well as the truth metric in [13] using lane width determination is presented. The test hardware can be seen in

Figure 3.10: Test Setup

in Figure 3.10, where the GPS antenna is mounted on the roof of the vehicle, the crossbow-IMU used is mounted in the center console, and the lidar is mounted on the roof rack with a web-cam attached to its front.

3.7 Results

The results shown in Figure 3.11 are those of experiments conducted at the NCAT test track, at a speed approximately 40 MPH. Due to a buffering issue with the lidar, only short tests with the lidar could be reliably preformed. The results show in Figure 3.11 are those compared to RTK truth data shown in red, and the lidar position data shown in green. The lidar data on average differs from the truth data by 0.0355m with a standard deviation of 0.0435m. This particular test is used as a metric of comparison to the tests preformed in

[13] which where of similar length where [13] attempted to driver perfectly straight for short sections and determine the accuracy of the algorithm's reported position, which was done with an accuracy of 0.25m.

Additional testing of increased duration were also preformed on the NCAT test track. The data presented in Figure 3.12 is of the vehicle making a single lap around the test rack under normal lighting and weather conditions. The mean absolute error was 0.1193m with a variance of 0.0546m. A distribution for this error can be seen in Figure 3.13. More extensive testing of the same scenario is presented in Figure 3.14, where multiple laps around the track are made. The mean absolute error for this test was 0.1305m with a variance of .0484m. A distribution of these errors can be seen in Figure 3.15. The specific stretch of track is one with a white solid lane marking to the right followed by a rumble strip, with white striped lane markings to the left.

In an effort to determine algorithm effectiveness, a number of tests where preformed in scenarios where an RTK truth solution could not be provided. In these circumstances however, the lane width was known, and therefore the data was analyzed to determine how well the lane width could be determined under various scenarios as well as how often lane markings where found. These metrics of success were chosen as a way of comparing this work to those methods presented in [23] and [13].

Scenario 1 is data gathered on highway conditions where a rumble strip borders the lane marking to the right. The right lane is solid and the left lane is dashed. The data from Scenario 1 is plotted in Figure 3.16, where the distance to the left and right lane markings with respect to the vehicle are shown. The algorithm is able to consistently track both solid and dashed lane markings with minimal position or lane width jumps. Scenario 2 is of a test where there is a double yellow lane marking to the left of the vehicle and a solid white lane marking on the right of the vehicle. Additionally, there is debris on the roadway in the form of gravel. Data from Scenario 2 can be seen in Figure 3.17, from which it should be noted that the gravel in the road posses a serious challenge. The left lane is only consistently

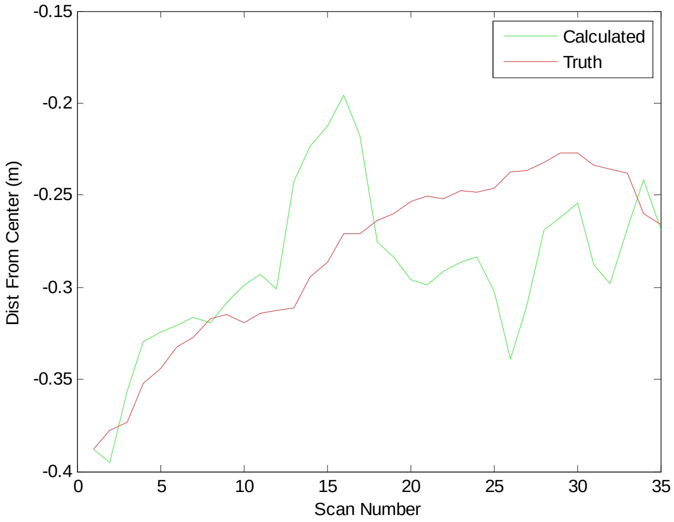

Figure 3.11: Lidar vs. Truth Data

tracked between scans 50 and 175, at which point the right lane is finally detected. Scenario 3 is on the same type of roadway as Scenario 2, but with the gravel now removed from the roadway but still present on the edges of the road near the lane markings. Results from Scenario 3 can be seen in Figure 3.18 where it should be noted that with the debris removed the lanes are able to be tracked much more consistently. However, the left lane tracker appears to have significant difficulty during scans 50-150 due to the debris closely bordering the lane markings. Finally, scenario 4 is a test of a solid yellow lane marking on the right and a solid white lane marking on the left. Grass closely borders both lane markings. Results form Scenario 4 can be seen in Figure 3.19 from which it is shown that the solid white lane marking is capable of being tracked much more consistently than the yellow lane marking. The results of lane width determination accuracy as well as detection rates are summarized in Table 3.3. These results are comparable to those presented in [23] and [13] where the maximum lane width error was $0.24m$ with a minimum detection rate of 16%.

Table 3.3: Results of Scenario Tests

	Avg. Lane Width Error (m)	Std of Error (m)	Detection (%)
Scenario 1	0.075	0.233	94.7
Scenario 2	0.042	0.272	81.7
Scenario 3	0.129	0.215	97.4
Scenario 4	0.169	0.329	76.86

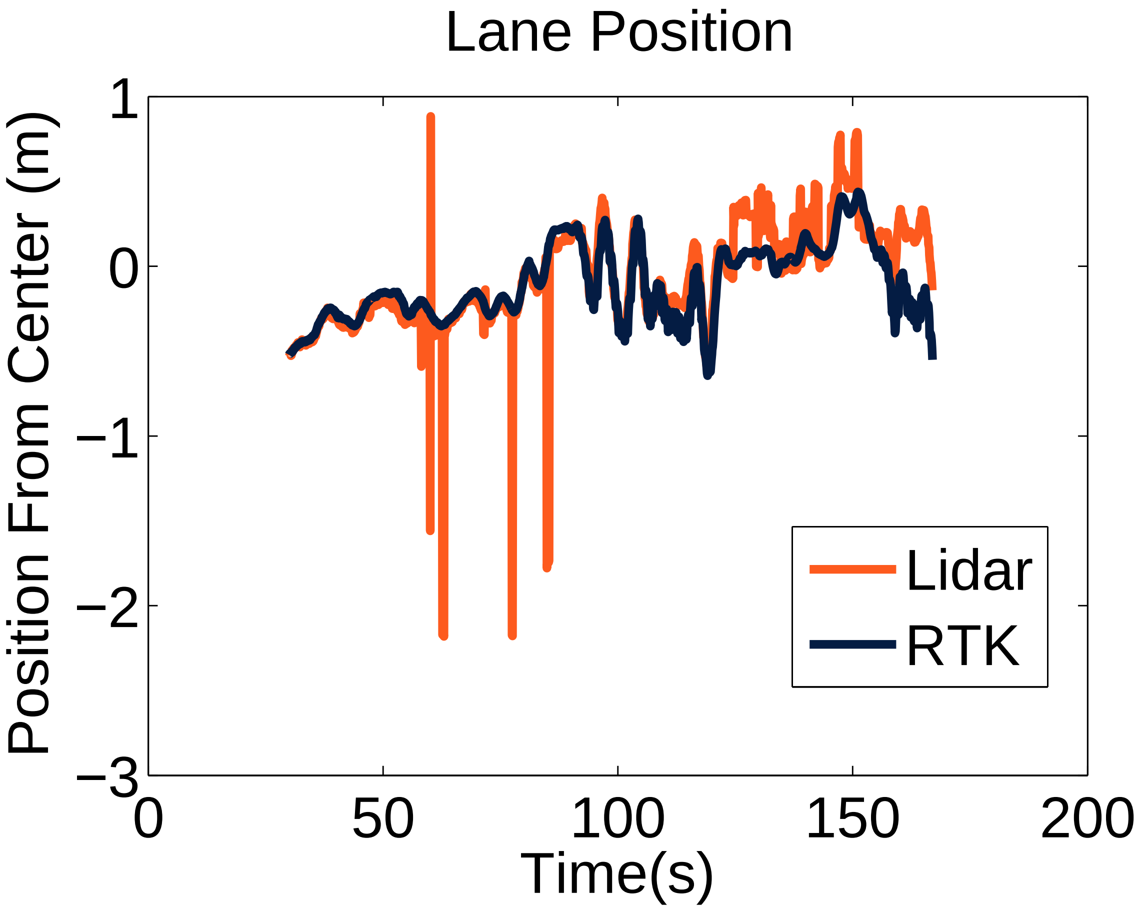

Figure 3.12: RTK Results Ideal Weather

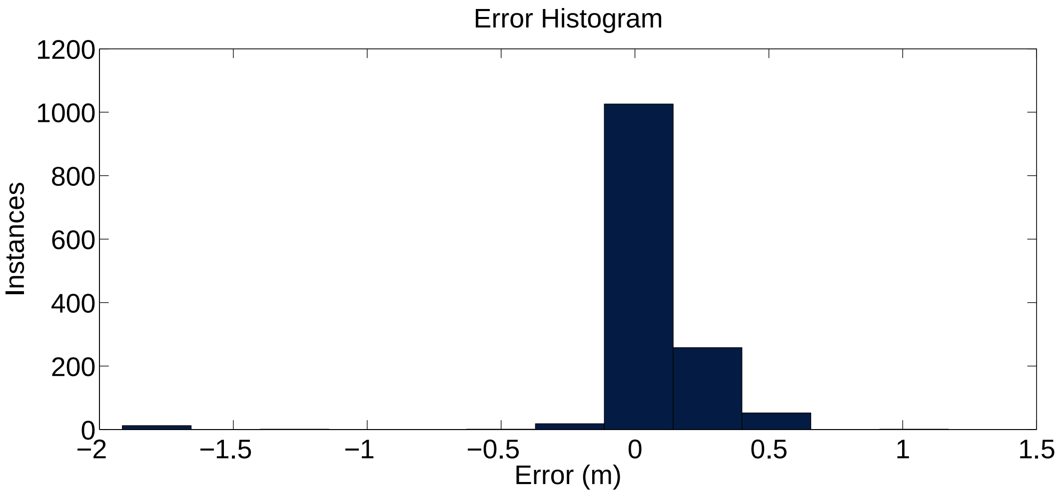

Figure 3.13: RTK Ideal Weather Error Distribution

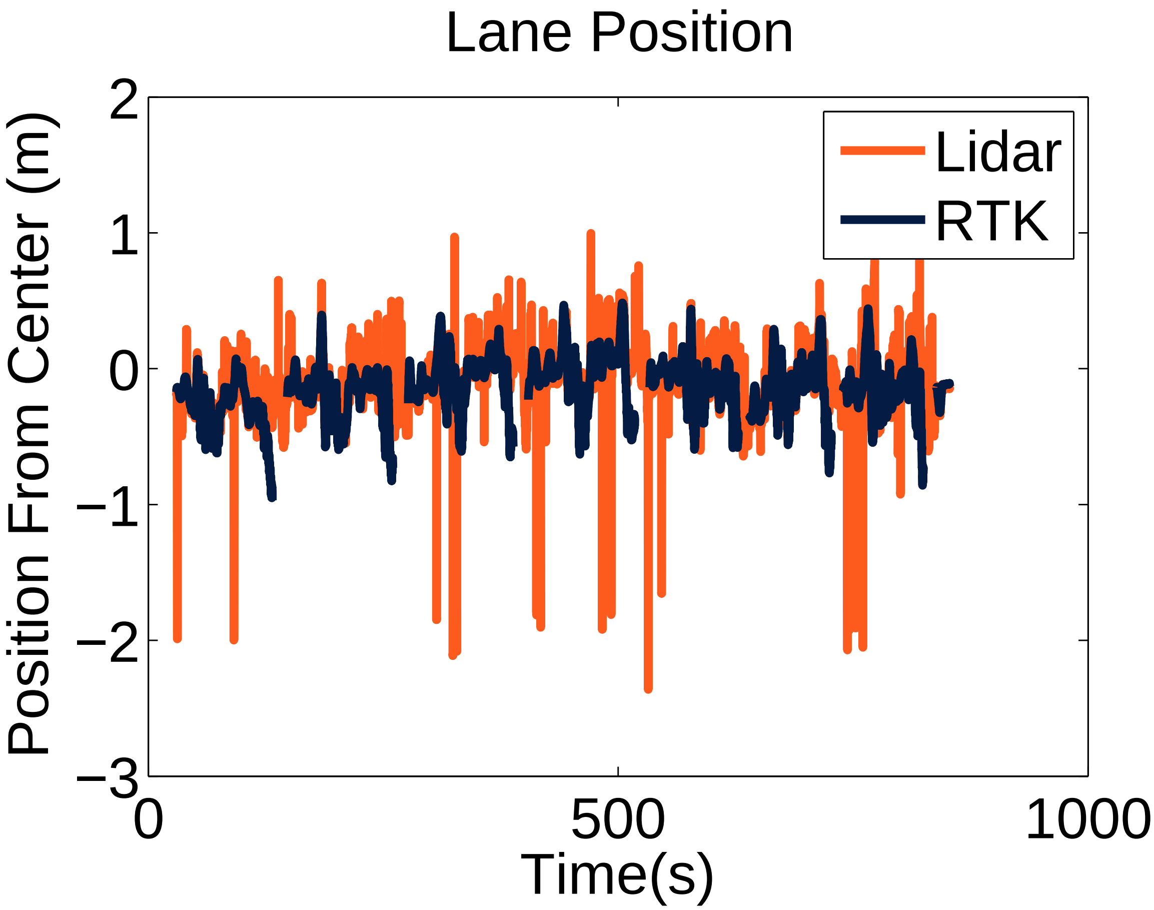

Figure 3.14: RTK Multiple Laps

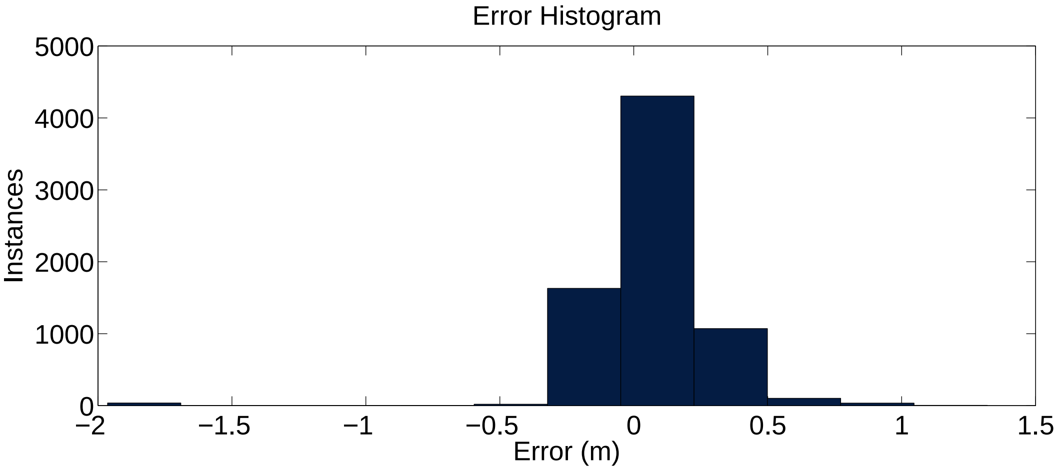

Figure 3.15: RTK Multiple Laps Error Distribution

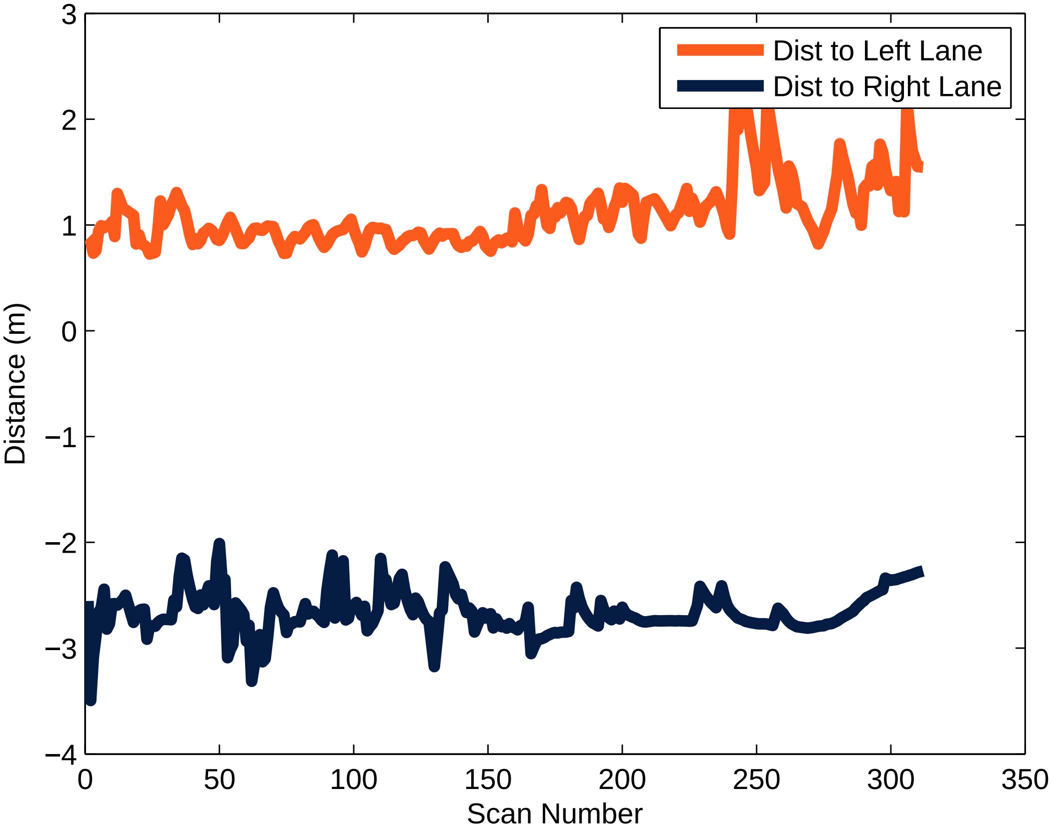

Figure 3.16: Scenario 1: Highway with Rumble strip on right, left lane solid, right lane is dashed

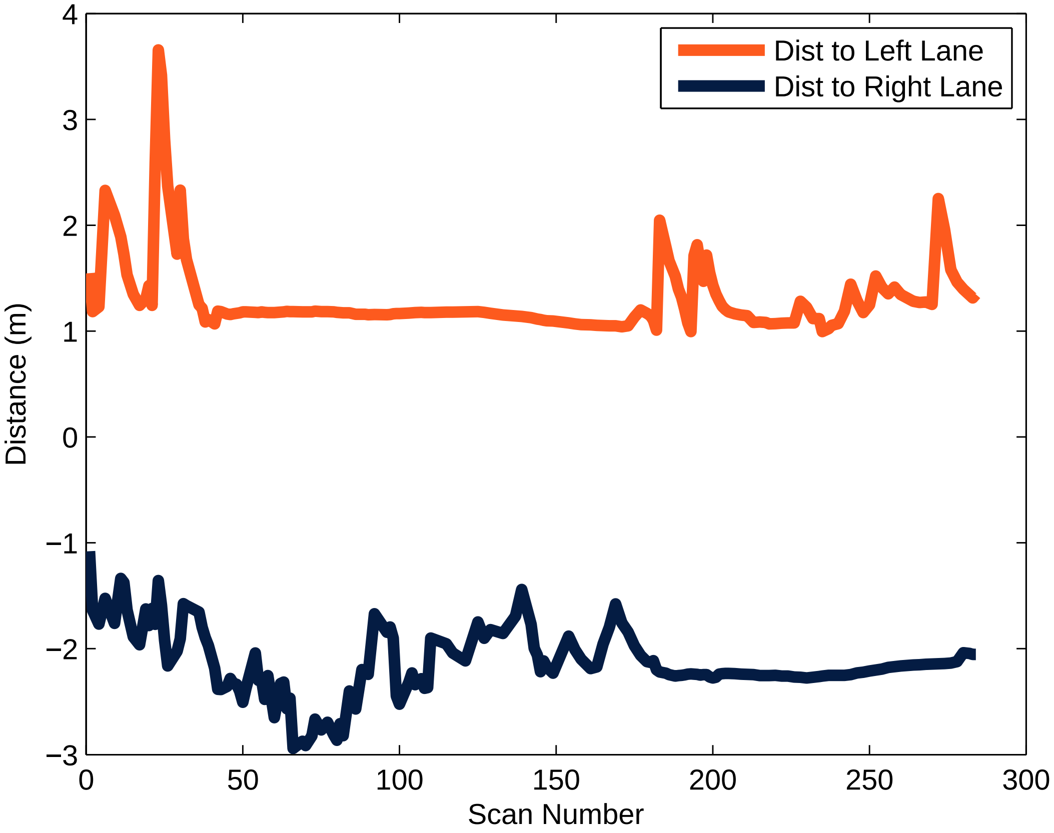

Figure 3.17: Scenario 2: Double yellow lines to left, solid white on right, debris in road

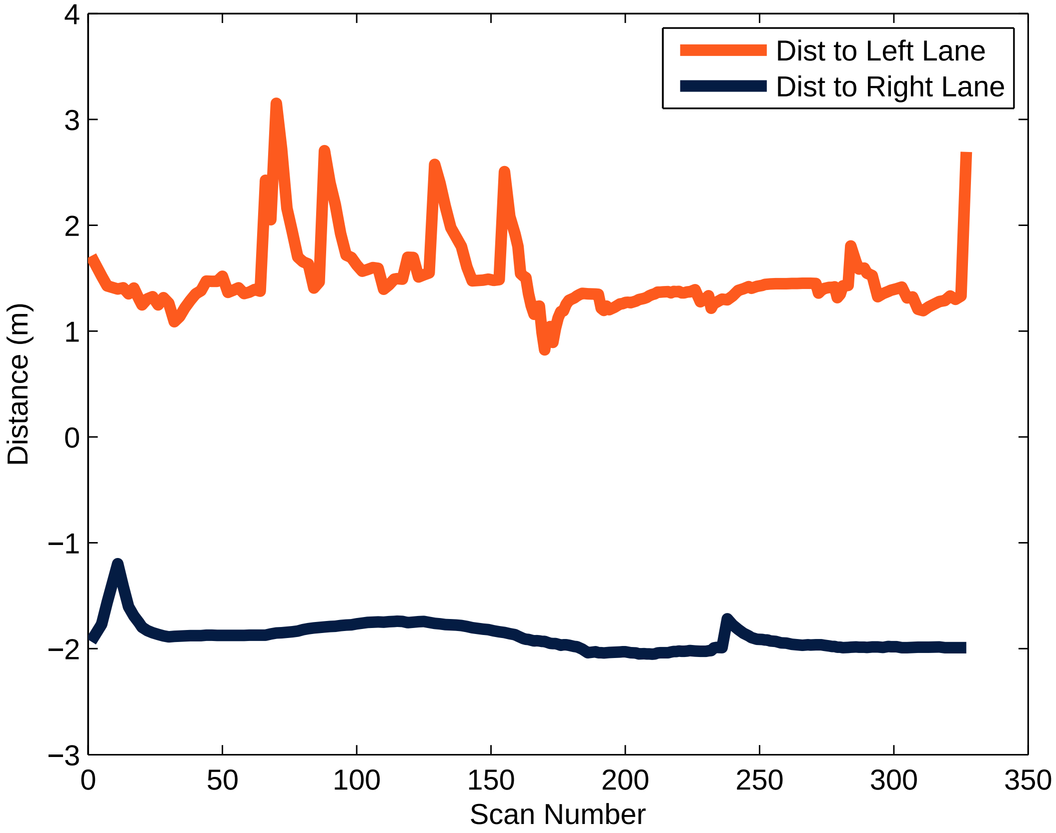

Figure 3.18: Scenario 3: Double yellow lines to left, solid white on right

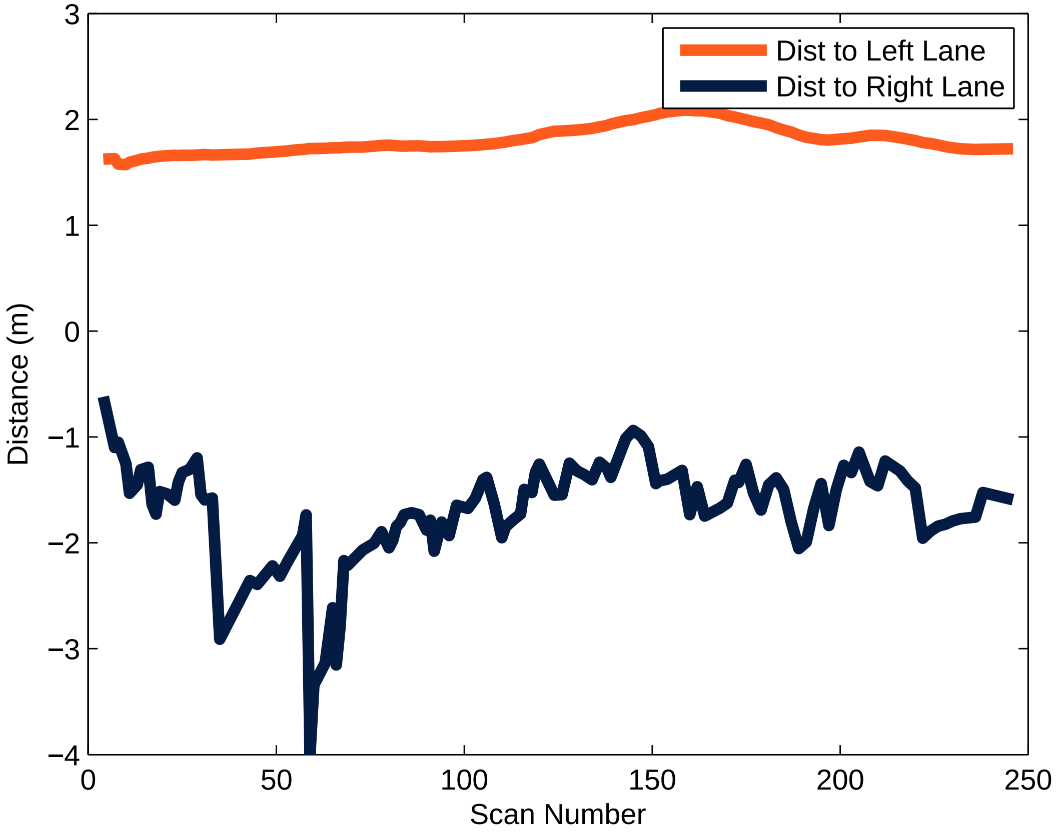

Figure 3.19: Scenario 4: Solid yellow on right, solid white on left, grass closely borders road

3.8 Conclusions

It would appear from the above results that the lidar is capable of locating the vehicle laterally in the lane to a distance comparable to that of a lane marking width. This work also presents a meaningful test metric not seen in literature by comparing results to an RTK survey of the lane markings. Additional work should include RTK results for different weather conditions, as well as future work in mitigating any errors with water on the roadway. It should be noted that grass bordering the roadway and debris on the roadway can present significant challenges to the lane extraction algorithm. Although data was not presented specifically for night driving, testing shows that changes in lighting conditions do not adversely affect the lidar.

Chapter 4

Lidar attitude estimation for vehicle safety systems

In applications involving lidar, especially for vehicle safety systems, it is crucial for the sensor to provide accurate and meaningful data. A lidar misaligned with the vehicle's axis or not properly accounting for changes in vehicle attitude can yield incorrect results. To combat these problems a number of lidar calibration techniques have been developed. Many of these techniques require the use of external hardware either in the form of a prior surveyed point [37, 32] or by scanning a known geometric structure [5, 27]. These lidar calibration techniques, while effective, do not easily lend themselves to a lidar system which must be calibrated in the filed. In contrast, the method developed here needs only a level plane in order to calibrate a multi-layer lidar to the vehicle's axis. Additionally, this technique can be used on vehicles to determine the vehicle's roll and pitch relative to a reference plane. Because this technique only needs a plane to calibrate to, it is thought that it will lend itself well to in the field calibration, where a garage, hanger, or smooth road should be available. Additionally, no complex maneuvers need to be accomplished, merely pitching the car, even by an unknown amount, is sufficient to calibrate the lidar. If this relative roll measurement is combined with inertial measurements, it could allow for the determination of what portion of vehicle roll is due to suspension deflection, and what portion is due to road bank. The solution presented is highly nonlinear and employs weighted recursive least squares as well as a high order unscented transform to deal with these non-linearities. A brief system overview is covered as well as specific nomenclature conventions for this algorithm. The derivation for this formula is presented as well as an overview of processing techniques used.

4.1 System and Nomenclature Overview

In the following algorithms it will be assumed that both the lidar and vehicle are operating in the north east down (NED) frame where the x-axis would be in the forward direction of travel for the vehicle and at $\gamma = 0°$ (as defined in section 3.2) for the lidar. Despite both the vehicle and lidar utilizing the same coordinate frame, the NED will denote a global coordinate frame and XYZ will denote the lidar coordinate frame in an effort to easily differentiate between coordinate frames. The yaw of the lidar relative to the vehicle is denoted as ψ (psi) as shown in Figure 4.1. The pitch of the lidar relative to a reference frame will be denoted as θ (theta) as shown in Figure 4.2. The roll of the lidar relative to a reference plane will be denoted as ϕ (phi) as shown in Figure 4.3. The pitch and roll of the vehicle relative to a reference plane will be denoted as λ (lambda) as shown in Figure 4.4 and ζ (zeta) as shown in Figure 4.5. The algorithm developed in this chapter makes no assumptions on the mounting location of the lidar other than that it is mounted in such a way where it is capable of scanning the road's or some other planar feature's surface

4.2 Derivation of Formula

In order to determine how the lidar is mounted relative to the vehicle the pitch, roll, and yaw of the lidar relative to the vehicle must be determined. Additionally, the vehicle pitch and roll will need to be determined, thus equations describing these unknowns relative to a plane are first derived. This method will assume that the vehicle is on a plane and initially experiences neither roll nor pitch relative to that plane. This method also assumes that the vehicle is capable of performing a pure pitch maneuver, i.e. that the vehicle is capable of pitching with no roll. Additional assumptions include that the vehicle is equipped with a forward looking 3-D lidar that is capable of making measurements to the plane that the vehicle is on, that all lidar measurements can be modeled as originating at the same physical location, and finally, that the lidar remains fixed on the vehicle once calibrated. Despite the

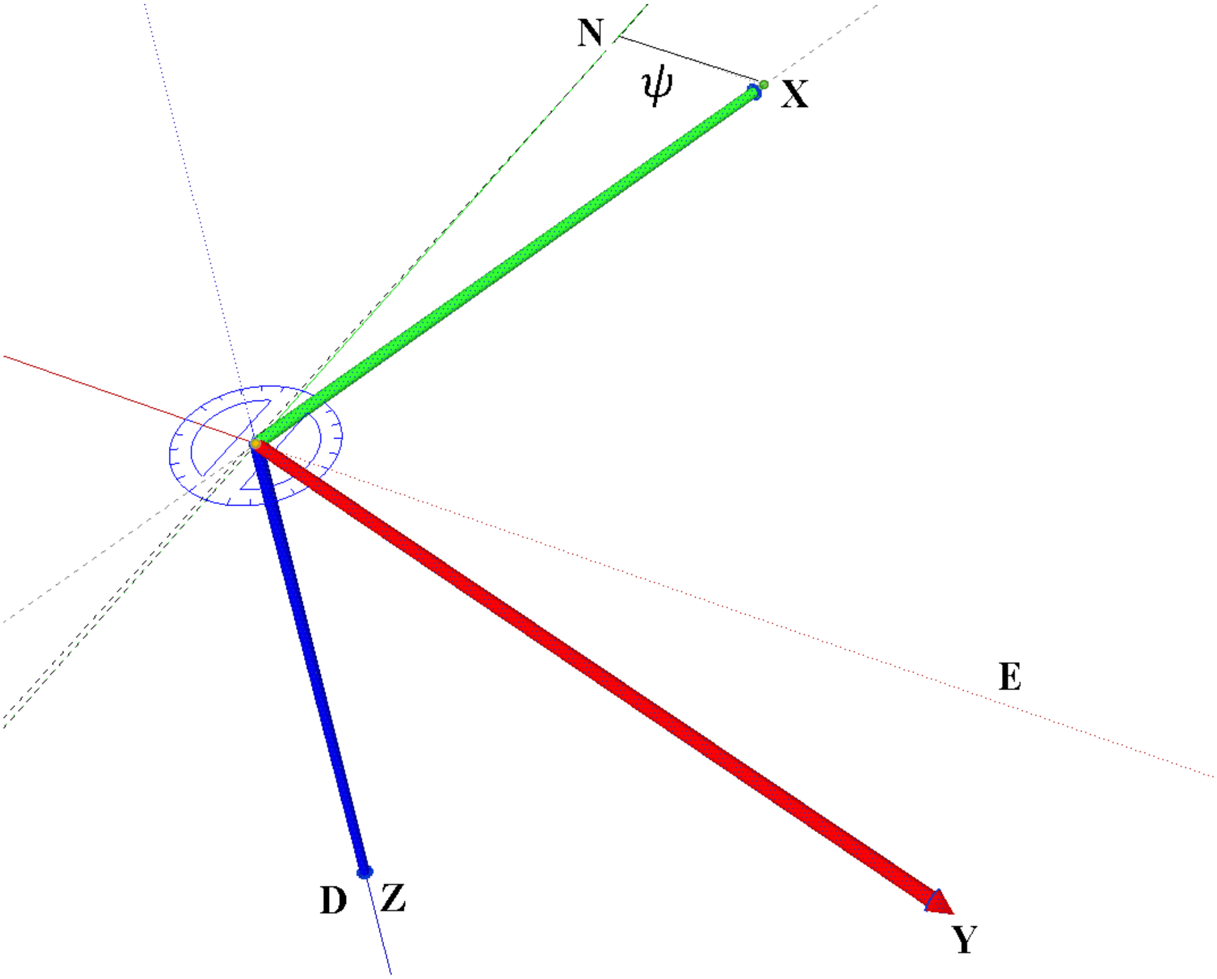

Figure 4.1: Relative Yaw

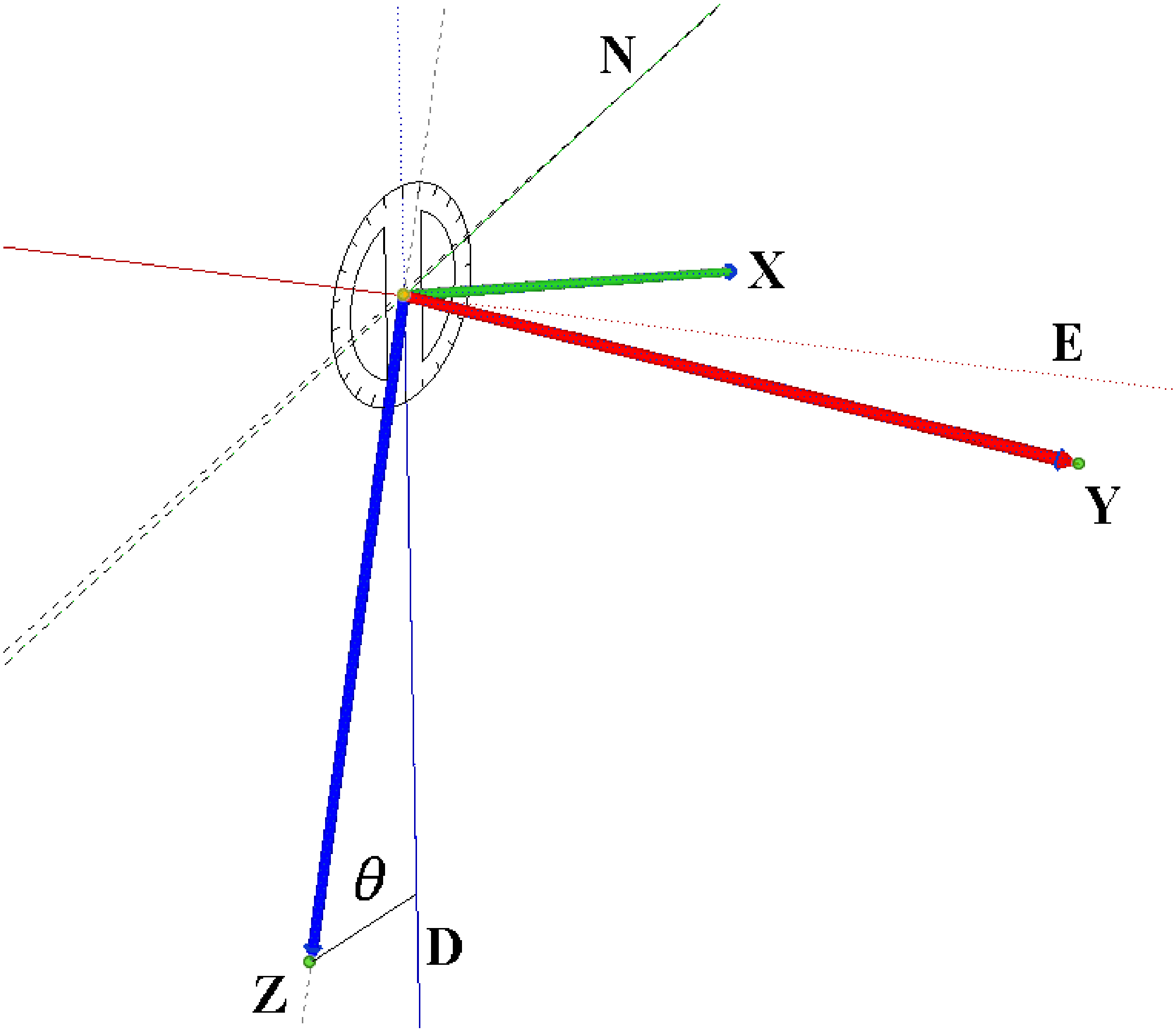

Figure 4.2: Lidar Pitch

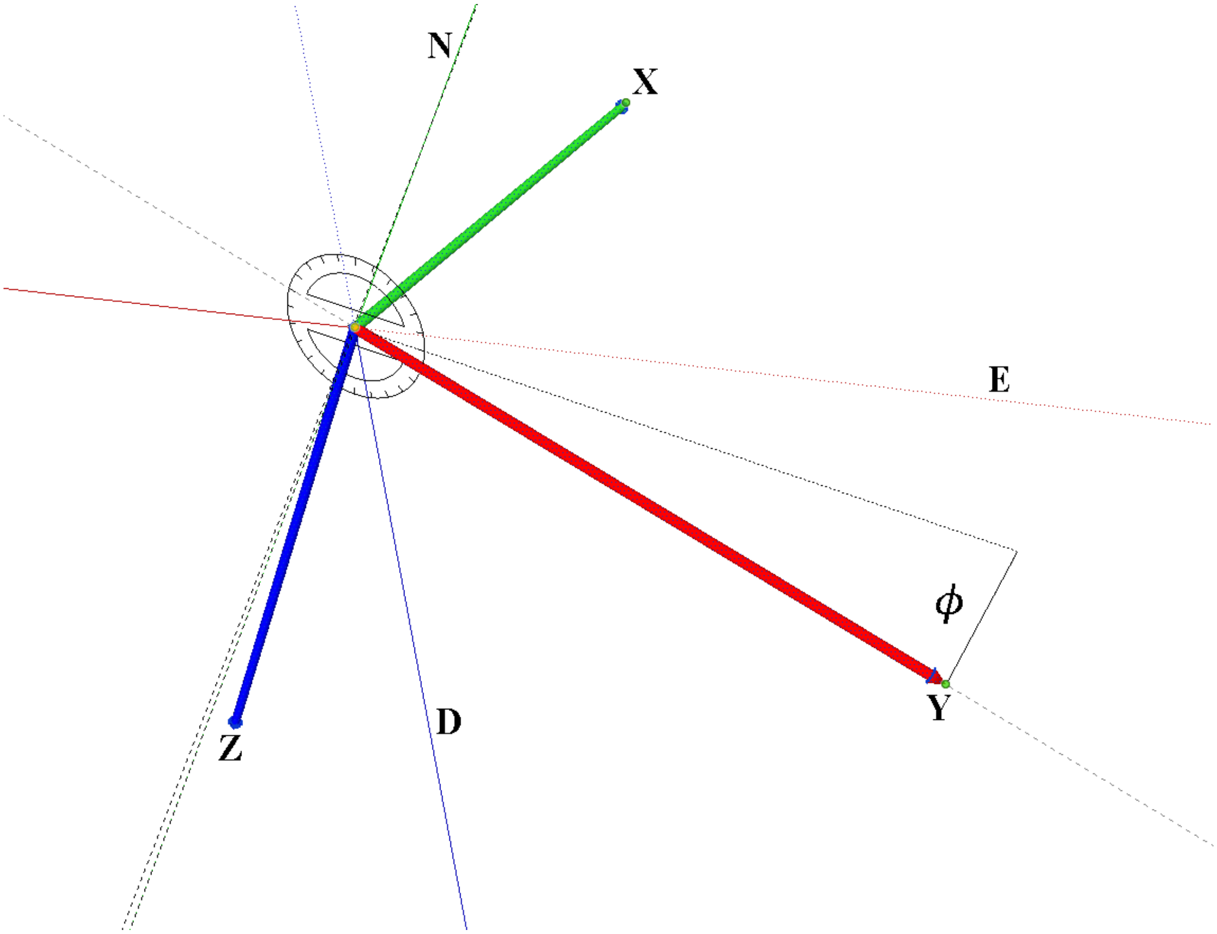

Figure 4.3: Lidar Roll

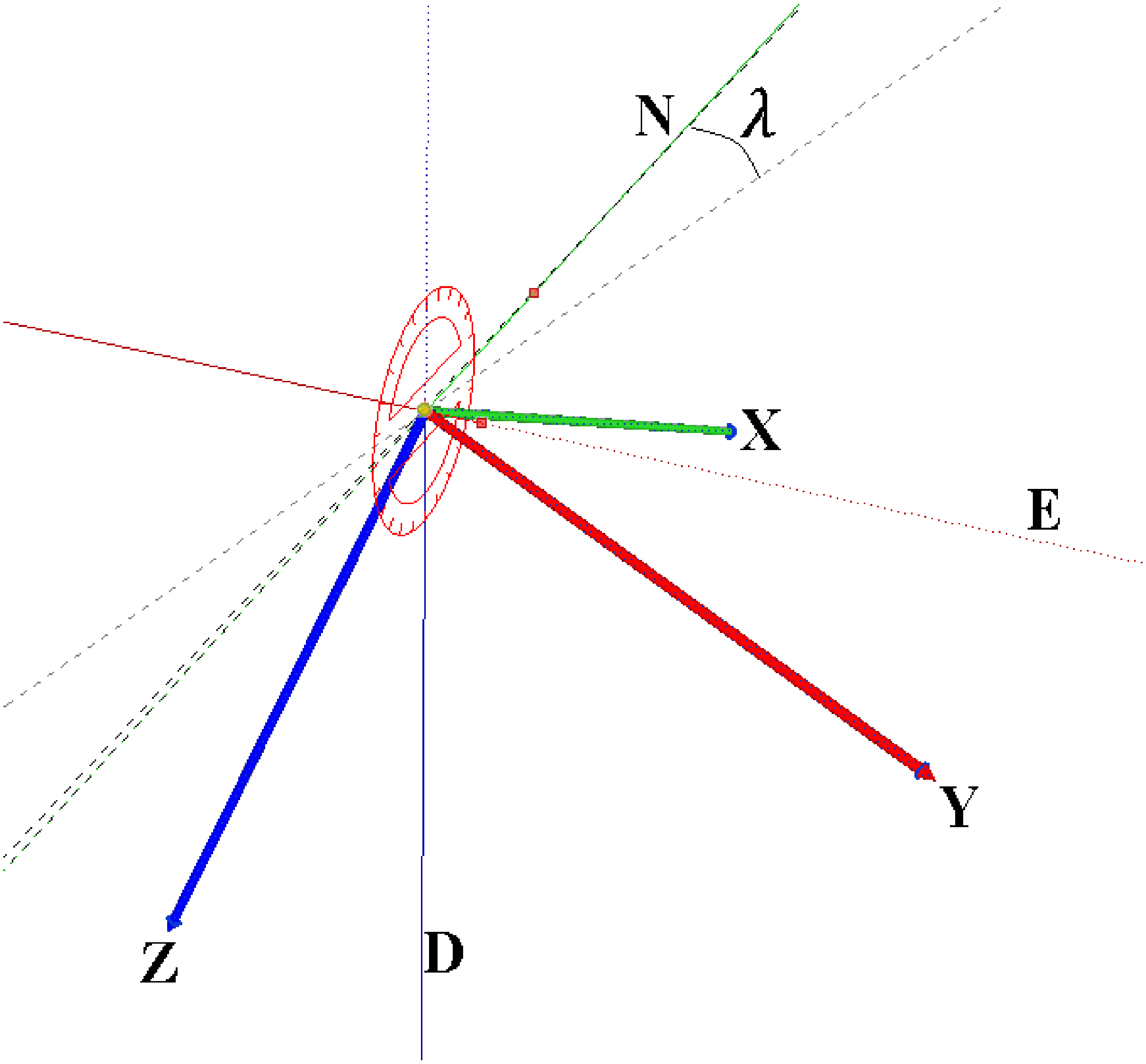

Figure 4.4: Vehicle Pitch

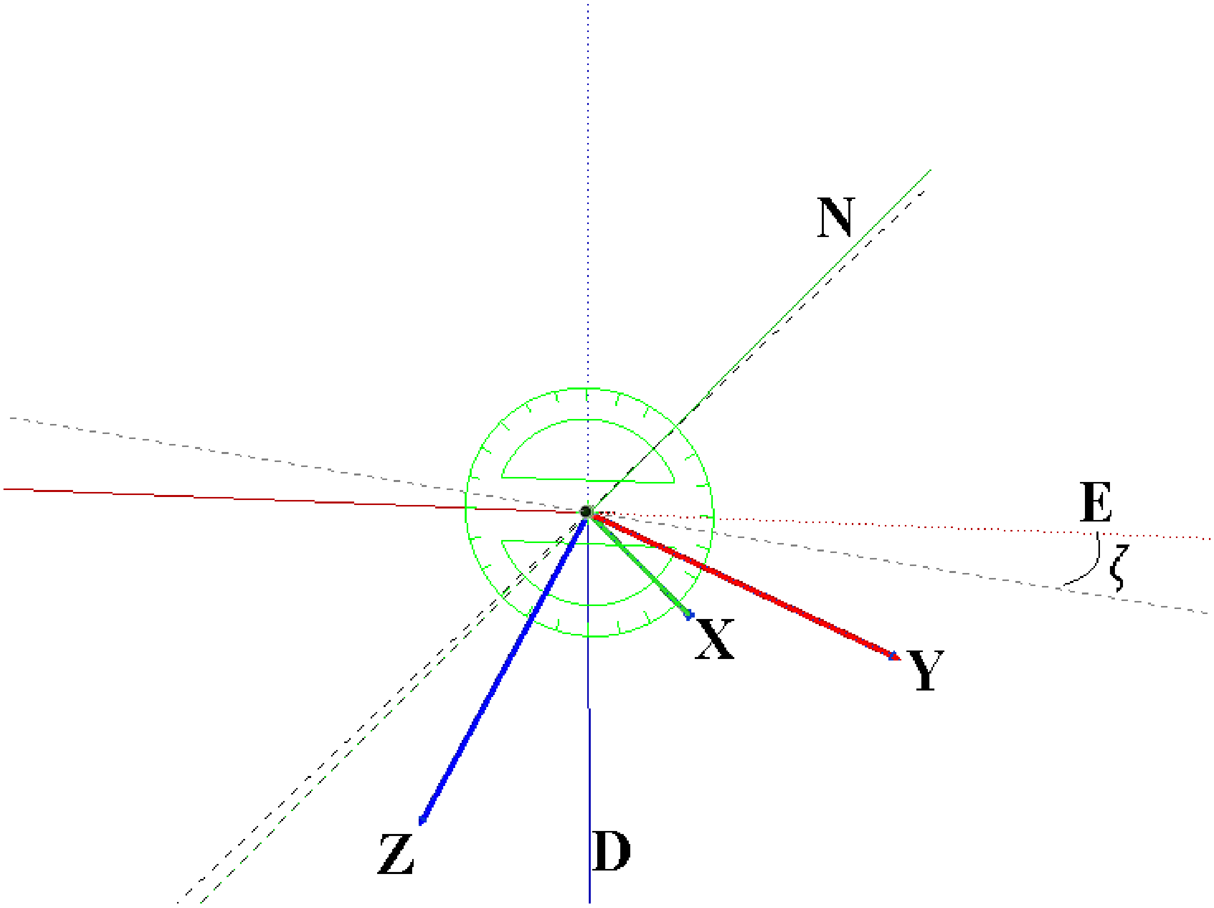

Figure 4.5: Vehicle Roll

lidar reporting measurements in a polar coordinate system, the following equations will adopt a Cartesian coordinate system in an effort to make the equations slightly more intuitive. The conversion used to convert the lidar measurements from a polar to a Cartesian coordinate frame is given in Equation(4.1) using the nomenclature established in section 3.2.

$$\begin{aligned} x_i &= \cos(\gamma_i)\cos(-\alpha_i) \\ y_i &= \sin(-\gamma_i)\cos(-\alpha_i) \\ z_i &= \sin(-\alpha_i) \end{aligned} \tag{4.1}$$

The equations describing the mounting error of the lidar relative to the vehicle, the lidar pitch, roll, and yaw, will be represented as body fixed rotations using Euler angles, where a right handed coordinate system is assumed. Therefore the order in which these rotations are preformed is important. The order adopted will be yaw, pitch, and then roll in an effort to conform to the standard order for many vehicle applications as presented in [15]. The system is initially modeled as both the lidar and vehicle having perfect alignment to the global coordinate frame. The lidar is then modeled as undergoing some change in yaw as shown in Figure 4.1 and represented mathematically in Equation(4.2).

$$\begin{bmatrix} N_i \\ E_i \\ D_i \end{bmatrix} = \left(\begin{bmatrix} \cos(\psi) & \sin(\psi) & 0 \\ -\sin(\psi) & \cos(\psi) & 0 \\ 0 & 0 & 1 \end{bmatrix} \right)^{\mathsf{T}} \begin{bmatrix} x_i \\ y_i \\ z_i \end{bmatrix} \tag{4.2}$$

The lidar is then modeled as undergoing a pitch dynamic as shown in Figure 4.2 and Equation(4.7).

$$\begin{bmatrix} N_i \\ E_i \\ D_i \end{bmatrix} = \left(\begin{bmatrix} \cos(\theta) & 0 & -\sin(\theta) \\ 0 & 1 & 0 \\ \sin(\theta) & 0 & \cos(\theta) \end{bmatrix} \begin{bmatrix} \cos(\psi) & \sin(\psi) & 0 \\ -\sin(\psi) & \cos(\psi) & 0 \\ 0 & 0 & 1 \end{bmatrix} \right)^{\mathsf{T}} \begin{bmatrix} x_i \\ y_i \\ z_i \end{bmatrix} \tag{4.3}$$

Note this will most likely be a negative number because the lidar is forward facing and needs to be facing the road's surface. The lidar is then modeled as undergoing some roll as shown in Figure 4.3 and Equation(4.4).

$$\begin{bmatrix} N_i \\ E_i \\ D_i \end{bmatrix} = \left(\begin{bmatrix} 1 & 0 & 0 \\ 0 & \cos(\phi) & \sin(\phi) \\ 0 & -\sin(\phi) & \cos(\phi) \end{bmatrix} \begin{bmatrix} \cos(\theta) & 0 & -\sin(\theta) \\ 0 & 1 & 0 \\ \sin(\theta) & 0 & \cos(\theta) \end{bmatrix} \begin{bmatrix} \cos(\psi) & \sin(\psi) & 0 \\ -\sin(\psi) & \cos(\psi) & 0 \\ 0 & 0 & 1 \end{bmatrix} \right)^{\mathsf{T}} \begin{bmatrix} x_i \\ y_i \\ z_i \end{bmatrix} \tag{4.4}$$

These equations describe the mounting of the lidar, where the pitch and roll is relative to a plane, and the yaw relative to the vehicle's axes. However, as shown in Appendice A, these equation can be used to solve for the lidar pitch and roll given any three non-collinear points. This is accomplished by using a previous assumption that all lidar measurements are originating at the same physical location, and therefore all measurements will have the same height. Hence, setting all D_i measurements from a single scan equal to one another will yield an over determined system. Note that the equation for D_i as seen in Equation(A.4) is not a function of yaw. This makes intuitive sense if one imagines the lidar perfectly level above a featureless plane. As the lidar rotates about its yaw axis, none of the lidar's measurements will change, and therefore this yaw value cannot be determined. Therefore the yaw of the lidar relative to the vehicle cannot be solved for directly and requires the vehicle to undergo an additional dynamic motion. The yaw of the lidar relative to the vehicle could also be determined with the addition of some feature in the environment be it retro-reflective tape or even a pole, however this would add an additional and unnecessary constraint to the algorithm.

Once the lidar's mounting pitch and roll has been calculated the lidar frame can be rotated so that it perfectly aligns with the vehicle's coordinate frame using Equation(4.4) if the yaw between the vehicle and lidar can be determined. This is accomplished using the argument that if the lidar and the vehicle's axes are perfectly aligned, then when the vehicle preforms a pure pitch maneuver, the attitude determination algorithm will measure no change in roll during this maneuver. If there is some change in roll between a static scan and a pitched scan, then this error is entirely due to some yaw between the lidar and the vehicle's axes. Thus, by comparing the roll measurement from a static scan and the roll measurement while the vehicle is undergoing some pitch maneuver, then the yaw of the lidar relative to the vehicle can be determined. Therefore equations describing vehicle pitch and roll must be determined.

Recall that Euler angles rotate only about a single axis, therefore a rotation matrix needs to be constructed to rotate about an arbitrary axis in reference to the lidar, which in this case would represent either the vehicle's pitch or roll axis. The rotation matrices that allows for a rotation about that arbitrary axis is shown in Equation(4.5) and Equation(4.6) using the notation developed in [15]. Note that Equation(4.5) is simply the rotation sequence developed in Equation(4.4), and Equation(4.6) is merely the rotation sequence that rotates measurements in the vehicle frame into the lidar's coordinate frame. Thus, these equations describe the rotations of the lidar's measurements into and out of alignment with the vehicle's coordinate frame. Now it is simply a matter of rotating the measurements about the vehicle's pitch axis as shown in Figure 4.4 and Equation(4.7). As well as the vehicle's roll axis is shown in Figure 4.5 and Equation(4.8).

$$R_b^g = \left(\begin{bmatrix} 1 & 0 & 0 \\ 0 & \cos(\phi) & \sin(\phi) \\ 0 & -\sin(\phi) & \cos(\phi) \end{bmatrix} \begin{bmatrix} \cos(\theta) & 0 & -\sin(\theta) \\ 0 & 1 & 0 \\ \sin(\theta) & 0 & \cos(\theta) \end{bmatrix} \begin{bmatrix} \cos(\psi) & \sin(\psi) & 0 \\ -\sin(\psi) & \cos(\psi) & 0 \\ 0 & 0 & 1 \end{bmatrix} \right)^{\mathsf{T}} \tag{4.5}$$

$$R_g^b = \left(\begin{bmatrix} 1 & 0 & 0 \\ 0 & \cos(\phi) & \sin(\phi) \\ 0 & -\sin(\phi) & \cos(\phi) \end{bmatrix} \begin{bmatrix} \cos(\theta) & 0 & -\sin(\theta) \\ 0 & 1 & 0 \\ \sin(\theta) & 0 & \cos(\theta) \end{bmatrix} \begin{bmatrix} \cos(\psi) & \sin(\psi) & 0 \\ -\sin(\psi) & \cos(\psi) & 0 \\ 0 & 0 & 1 \end{bmatrix} \right) \tag{4.6}$$

$$R_\lambda = \begin{bmatrix} \cos(\lambda) & 0 & -\sin(\lambda) \\ 0 & 1 & 0 \\ \sin(\lambda) & 0 & \cos(\lambda) \end{bmatrix} \tag{4.7}$$

$$R_\zeta = \begin{bmatrix} 1 & 0 & 0 \\ 0 & \cos(\zeta) & \sin(\zeta) \\ 0 & -\sin(\zeta) & \cos(\zeta) \end{bmatrix} \tag{4.8}$$

The full equation for compensating for both lidar yaw, pitch, and roll due to a mounting error as well as vehicle pitch and roll, is given in Equation(4.9), which simply rotates the lidar's measurements from the lidar frame to the vehicle frame by first compensating for the lidar's mounting error, and then compensating for vehicle roll and pitch. As noted previously, all D_i measurements, shown in Appendix A, for a single scan are equal to one another and can be used to determine vehicle pitch as shown in Appendix B and C as well as roll, as seen in Appendix D. By comparing the roll measurement of a static lidar scan and the scan of a lidar while preforming a pure pitch maneuver, the yaw of the lidar relative to the vehicle can be determined as shown in Appendix E.

$$\begin{bmatrix} N_i \\ E_i \\ D_i \end{bmatrix} = R_b^g R_b^g R_\lambda^\intercal R_\zeta^\intercal R_b^g R_g^b R_b^g \begin{bmatrix} x_i \\ y_i \\ z_i \end{bmatrix} = R_\lambda^\intercal R_\zeta^\intercal R_b^g \begin{bmatrix} x_i \\ y_i \\ z_i \end{bmatrix} \tag{4.9}$$

It should be noted here that this algorithm does posses a singularity for pitch at -90° which should be avoided in both mounting and when pitching the vehicle. Additionally, when calibrating the lidar, the larger the change in pitch between the static and dynamic scan the better the calibration result (as this will reduce the affects of any noise on the system). Additionally, it is possible to obtain inaccurate results for calibration while still obtaining meaningful results for attitude. This case occurs when the vehicle is on a plane, but the vehicle is not aligned with the plane. Such would be the case if the car where experiencing some constant roll or pitch due to the weight of the driver. The lidar will report its mounting angle relative to the ground plane, but this would not necessarily correspond to the mounting of the vehicle. However, because the algorithm aligns the lidar's axes to the vehicles through the pure pitch maneuver the correct change in vehicle attitude can still be computed, because it is the change between static and dynamic scans that is analyzed. Once again, a 3D lidar must be used for these calculations. This is because these algorithms essentially require that a plane be defined so that pitch and roll relative to that plane can be determined. Because 2D lidars take a slice of the environment, all points are co-linear, and therefore a plane cannot be defined, and consequently, these equations will not compute a meaningful answer.

4.3 Processing data

Data is processed in such a way that the mounting roll is found first followed by the mounting pitch. Once these are obtained the yaw offset can be calculated. Finally the dynamic roll and dynamic pitch are calculated. Because of the large amount of data that can be provided by the lidar, the particular method in which data is selected and processed can be critical for real-time applications. This is especially clear when attempting to calculate the yaw offset. This is because while the calculations for pitch and roll are simply attempting to define a certain value as defined by some plane, the yaw offset calculation is attempting to compare two planes. Thus, there are lidar scans from both the static and dynamic scans need to be processed. Hence if P represents a group of xyz coordinates there would be six groups of P, three for the first plane, and three for the second. If an exhaustive processing scheme where desired, this would mean that the first set of P points were iterated through while the other were held constant, and so on, until every possible combination of planes had been analyzed. Thus, the processing scheme would be on the complexity of $O(n^6)$. On the machine that this data was processed over for 50 scans, it would require over a week to determine the yaw of the lidar relative to the vehicle. An alternative method was found by simply iterating through all sets of P at the same time, thus providing an algorithm on the complexity on the order of $O(n)$. While this is not as exhaustive of a result as the previous method, it is significantly less cumbersome to process. The pitch and roll measurements are also processed in this way giving them a computational complexity on the order of $O(n)$, whereas they would be on the order of $O(n^3)$ otherwise.

Additionally, when processing pitch, not all points need be processed. Due to the geometry of the lidar scan on the planar surface it is possible that some of the points taken will have significantly more variation in the X direction, than others. Those with little variation in the X direction should not be processed, because the event of no variation in the X direction is a mathematical singularity for the pitch calculation. For the roll calculation, it is ideal for the scanned points to have as much separation between them as possible to avoid any mathematical singularities. However, as long as these points define a plane, no mathematical singularity will be reached.

4.4 Higher Order Unscented Transform (HOUF)

It is necessary to develop a transformation that transforms the uncertainties in the lidar measurements to an uncertainty in an attitude measurement. Developing this transformation to be capable of accurately transforming a highly nonlinear equation can be difficult because often, the transformed distribution cannot be described with a finite number of parameters [1]. Such is the case when the transformation is approximated through linearization, where the higher order terms of a Taylor series expansion are truncated, often to the first order. In contrast, the higher order unscented transform attempts to approximate a probability distribution rather than a non-linear transformation. This is accomplished by creating a set of weighted samples that capture the mean, covariance, and kurtosis of the prior distribution. The non-linear function is then applied to each one of these weighted samples from the prior distribution to yield a cloud of transformed samples. This allows higher order information to be captured, in this case, up to the eighth order moment, with a small number of points. This is done using Equations (4.10-4.19), as derived in [1, 20]. Where assuming some nonlinear function of the form $F = g(X)$ with variance P_x, Equations(4.10) and (4.11) represent the sigma-set which will exhibit the statics of X.

$$\zeta_0 = \bar{X} \tag{4.10}$$

$$\begin{gathered} \zeta_i = \zeta_0 + \sigma_i \\ \text{for}\, \sigma_i = \pm\sigma_1, \pm\sigma_2 \end{gathered} \tag{4.11}$$

Where $\sigma_1$and σ_2 are defined in Equations(4.12) and (4.13).

$$\sigma_1 = (5 + \sqrt{10})\frac{P_x}{3} \tag{4.12}$$

$$\sigma_2 = (5 - \sqrt{10})\frac{P_x}{3} \tag{4.13}$$

The weights for the transformed sigma-set are defined in Equations(4.14-4.16)

$$w_0 = 1 - 2(w_1 + w_2) \tag{4.14}$$

$$w_1 = \frac{P_x(P_x - \sigma_2^2)}{6\sigma_1^2(\sigma_1^2 - \sigma_2^2)} \tag{4.15}$$

$$w2 = \frac{P_x(\sigma_1^2 - P_x)}{6\sigma_2^2(\sigma_1^2 - \sigma_2^2)} \tag{4.16}$$

The sigma-set is this transformed by the given non-linear function as shown in the following equations.

$$\eta_i = g(\zeta_i) \tag{4.17}$$

$$\bar{\eta} = \sum w_i \eta_i \tag{4.18}$$

$$\mu_\zeta^j = \sum w_i (\eta_i - \bar{\eta})^j \tag{4.19}$$

Where $\bar{\eta}$ represents the mean of the transformed function, η_ζ^j represents the j^{th} central moment of the transformed function.

4.5 Least Squares (LS) / 1 state Kalman Filter (KF)

Instead of taking a more standard approach and processing these algorithms results using weighted or batch least squares such as in [38, 28], a single state Kalman filter was used. The single state Kalman filter was used over weighted least squares simply because it showed marginally better results due to tuning. The equations for the Kalman filter introduced previously in Equations(3.12-3.16), where the single state is the attitude measurement currently being calculated. The measurement noise used is obtained from the HOUF. The process uncertainty measurement P, is propagated to future attitude calculations as a metric of the accuracy of a previous attitude calculation.

4.6 Conclusions

This chapter has presented the equations necessary to determine the mounting pitch and roll of a lidar to a plane, as well as the relative roll between the vehicle and the lidar. Additionally, this chapter has presented the equations necessary to determine the vehicle's pitch and roll relative to a plane. An overview of processing complexity has been presented as well as the techniques used to process the data.

Chapter 5

Lidar Attitude Estimation Testing

This chapter presents attitude tests to determine the performance of the lidar attitude system in both in-door benign tests as well as in outdoor dynamic tests. The static tests were preformed in a hallway and the dynamic tests were preformed atop of a parking garage as well as on a skid pad.

5.1 Static Testing

Testing for the static tests were preformed in a hallway in order to both mimic the limited field of view a laser scanner might have when scanning a road, as well as to use the floor as a planar surface. A three degree of freedom jig was created so that the the lidar could be simulated undergoing both vehicle pitch and roll maneuvers independently, as well as having some yaw with respect to the vehicle. The lidar, even with no yaw error, was still offset from the vehicle's pitch and roll axes, however this difference could not be directly altered on test device. The base of this actuation device will be considered analogous to the vehicle's frame for the following tests.

5.1.1 Test Procedure

The lidar was mounted on the test device approximately 1m off the floor with some initial pitch, roll, and yaw error with respect to the vehicle axes. This initial pitch, roll and yaw offset was held constant for the following tests. Note that no attempt was made to assure the jig's base was perfectly aligned to the plane defined by the floor. An initial scan of the hallway floor was taken and the mounting pitch and roll of the lidar was determined. The lidar then underwent a pure vehicle pitch maneuver, and data was again recorded. The data from the static scan and the scan from the pitch maneuver where then compared to determine the yaw offset. This yaw offset, mounting pitch, and mounting roll were used for all following calculations. The lidar then underwent various vehicle pitch and roll maneuvers. Some maneuvers involved only changes in pitch, others changes only roll, and some involving changes in both axes. Data was taken only while the lidar was static. This was done so that multiple lidar scans could be taken at the same physical location as well as provide enough time for the truth measurement to be read and recorded. Truth measurements were provided by an inclinometer. Because the tests where comparing only the change in angle between various test positions simulating vehicle dynamics, the inclinometer's value was recorded with each new position. Hence the change in inclinometer reading between two test positions served as the truth value which the attitude determination algorithm would be compared against.

5.1.2 Hardware Overview

The laser scanner used for these test was the same lidar presented in Section 3.1 (an Ibeo ALASCA XT). This lidar was chosen because it is capable of measuring in all three dimensions as well as all measurements from the lidar can be accurately modeled as originating at the same physical location, which allowed us to meet the necessary assumptions made for this algorithm as presented in section 4.2. The sensor used to collect vehicle pitch and roll truth data was a T6 incremental inclinometer made by USDIGITAL, which was capable of measuring an angular change to within an accuracy of 0.1°. Note that these sensors are measuring an absolute angle not an Euler angle which must be compensated for. Additionally, despite the inclinometers being capable of measuring angular change to within 0.1° the jig on which the lidar was attached was not constructed to this tolerance. Therefore the jig will most likely have some amount of compliance between pitch and roll axes. Finally, no additional sensors were used to confirm the results gathered during the calibration phase.

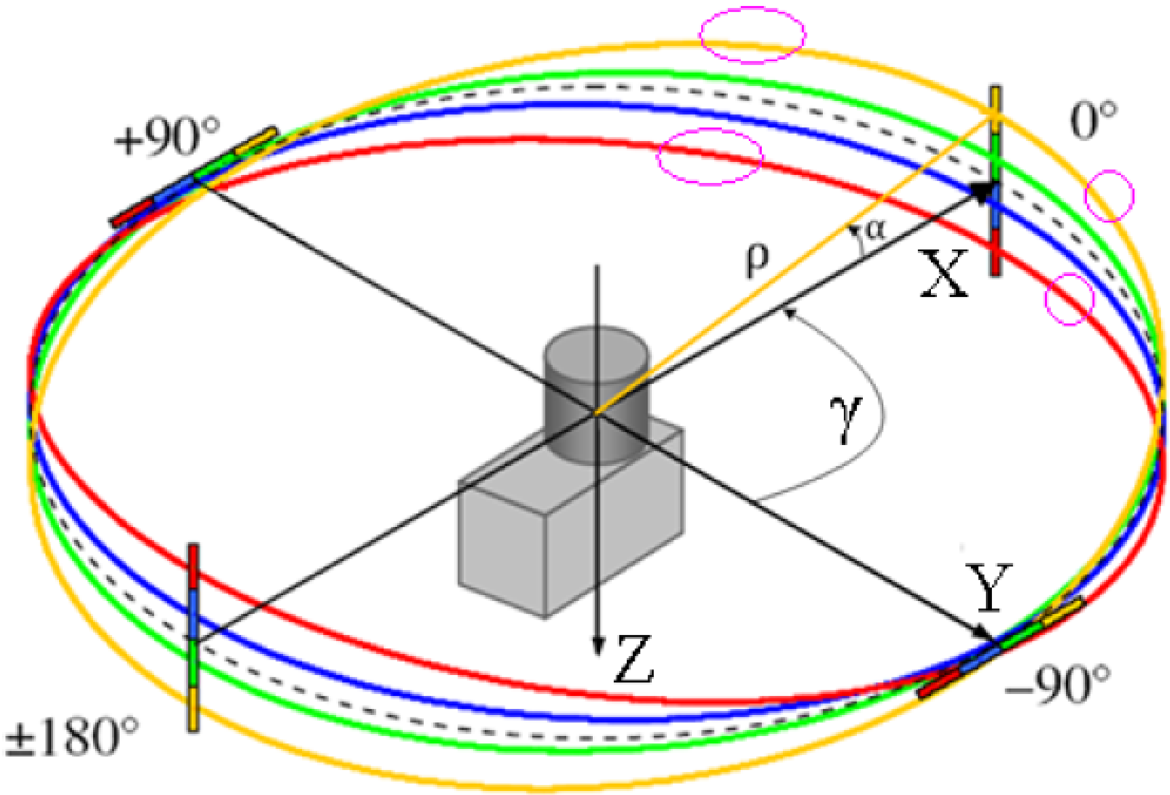

Figure 5.1: Location of lidar data processed

5.1.3 Data Selection and Processing

In an effort to simulate an in-the filed test where an operator may not have an extremely large time budget for calibration or attitude determination, not all of the lidar scan data was processed. Data was selected from the upper most layer, and bottom most layer at angles between 35° and 25°, and -35° and -25°, which constituted approximately eighty lidar measurements per scan. This can be seen graphically in Figure 5.1 where the locations from which data was taken are represented as magenta ovals. Approximately fifty scans per test position were taken.

These data points were then divided into three groups. Group one was data from layer A at an angle of 35° to 25°, group two was data from layer A at angle of -35° to -25°, and layer three comprises data from layer D from angles 35° to 25° and angles -35° to -25°. Data was processed in such a way so that each point in a single group was compared to every other point belonging to a different group. Hence, for calibrating roll, a set of three nested for loops were constructed such that a single point from group one was compared to all combinations of points in groups two and three.

The results reported by the algorithm for vehicle pitch and roll needed to be compensated for before comparing to the inclinometer results because the lidar based algorithm is reporting Euler angles while the inclinometers are reporting absolute angles. Therefore, once results for the lidar based algorithm were obtained, a series of projections were preformed. The first projection was used to find the absolute pitch. Hence a vector of arbitrary length in the x_i direction was created and rotated using Equation(4.9), and the results of the lidar based algorithm. The angle that this projection made with the N and D axes of the global frame was taken to be the absolute pitch and was compared to the inclinometer's reading. A similar technique was used to find the global roll, however the arbitrary length vector is now in the y_i direction and the angle between the E and D axes of the global frame was taken to be the absolute roll.

5.1.4 Results

The results presented here are from the comparison of the absolute pitch and roll derived by projecting the resulting Euler angles determined by the lidar attitude estimation algorithm and the absolute angles reported by the inclinometers. Specifically, these tests compare the reported change in attitude from the lidar between two scan points and the reported change in attitude from the inclinometers. It should be noted that there were no sensors used to confirm the calibration aspect of the algorithm. However the vehicle pitch and roll estimates should include both errors in calibration as well as attitude estimation.

Roughly 200 tests were preformed using 20 unique calibration points. The vehicle pitch varies from 352.5° to 340.8°, and roll varies between 0.1° and 337.1°. The pitch and roll results from one round of these tests can be seen in Figures 5.2 and 5.3. Additionally, a histogram of the errors for all 200 tests are presented in Figure 5.4.

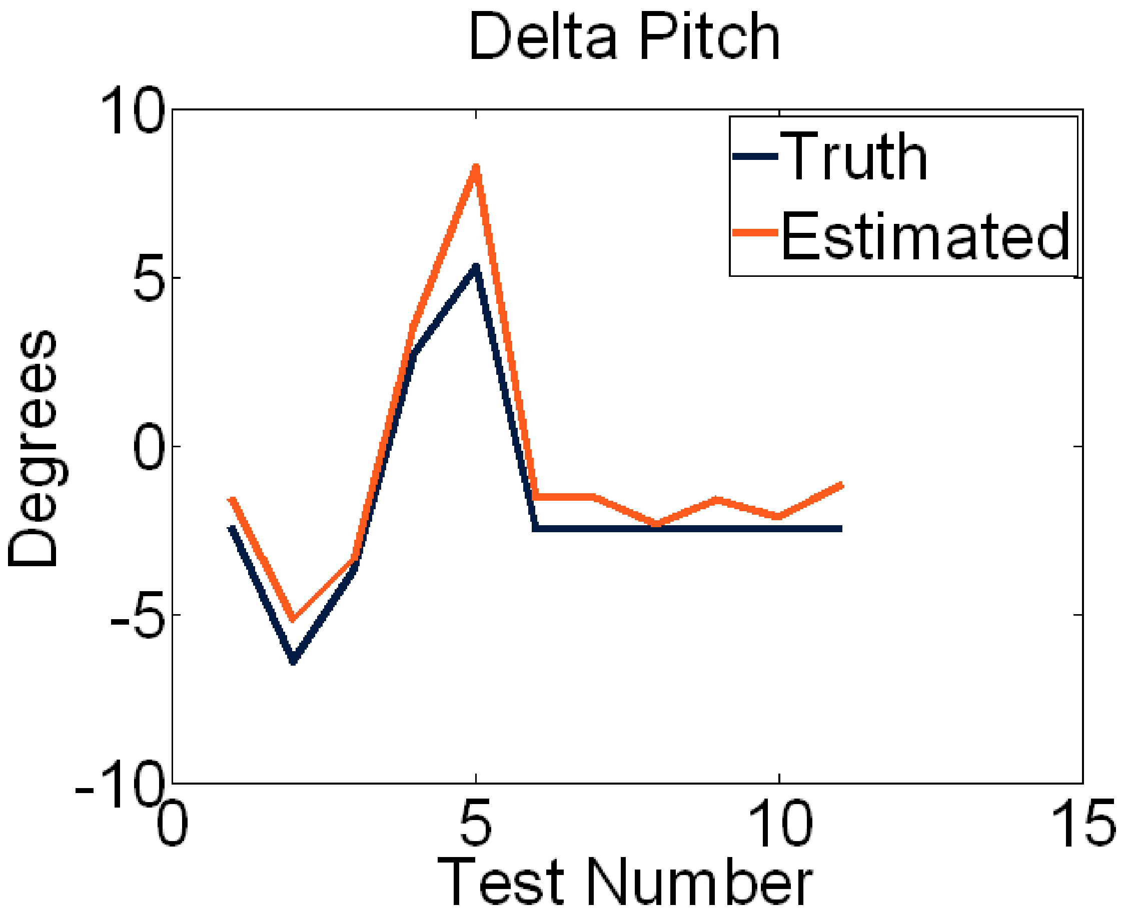

Figure 5.2: Delta Vehicle Pitch

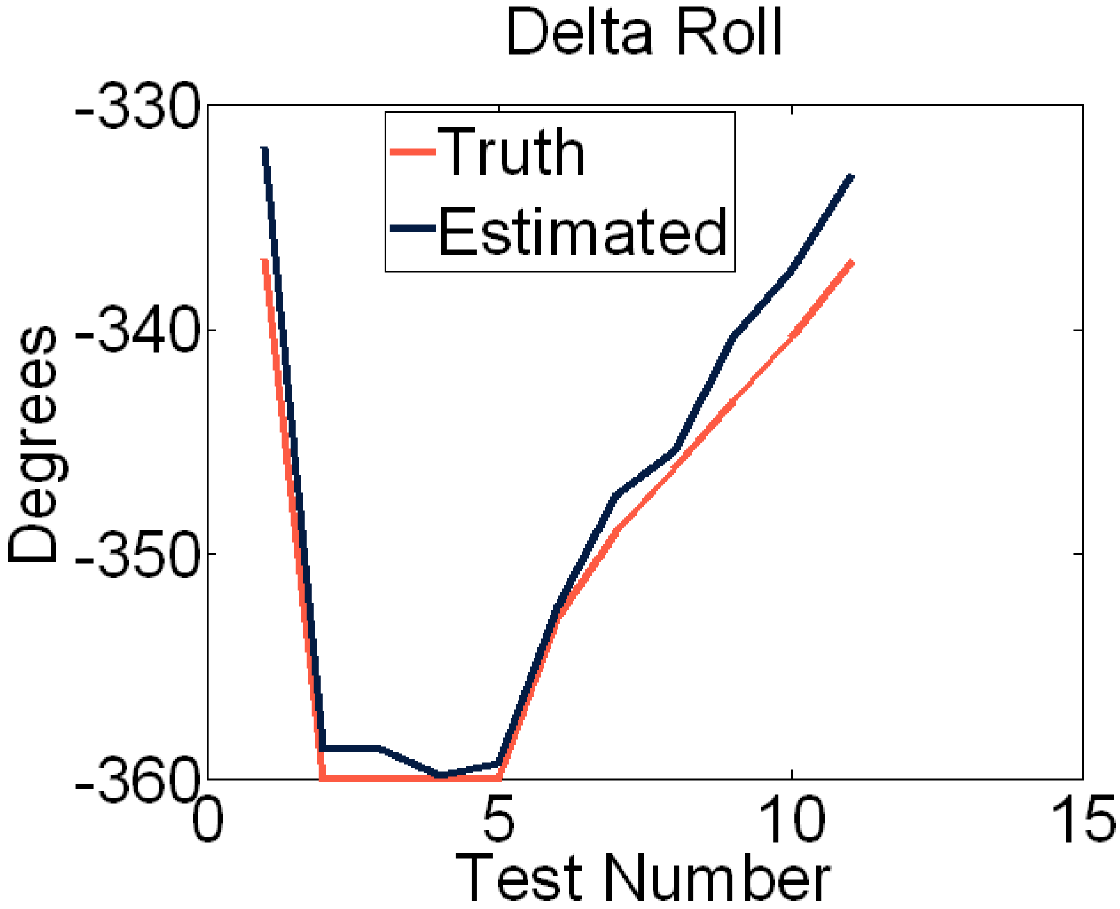

Figure 5.3: Delta Vehicle Roll

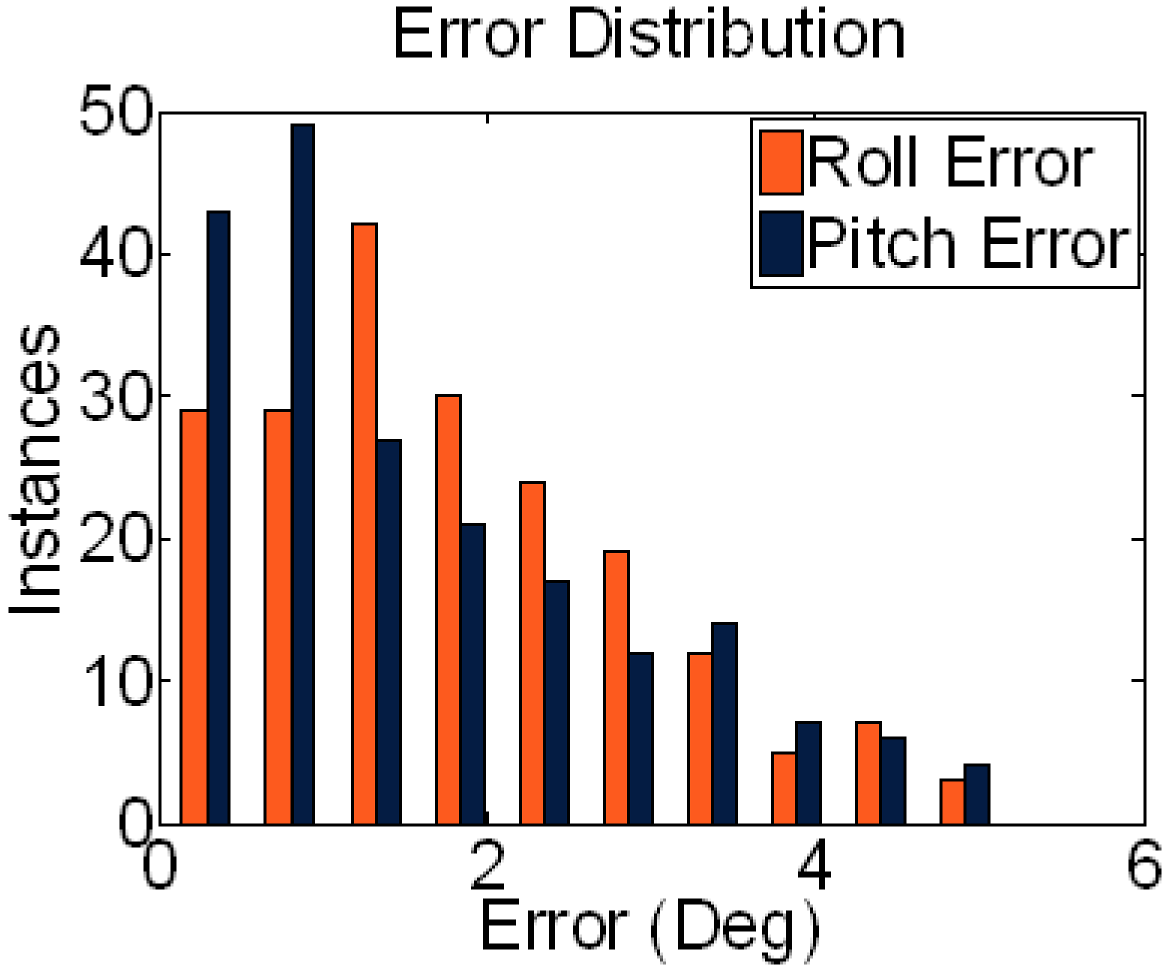

Figure 5.4: Histogram of Pitch and Roll Errors

5.2 Dynamic Testing

Dynamic tests were preformed on the roof of a parking garage. This location was chosen because it was thought that the driving surface would adequately approximate a plane. Additionally it would provide a clear and unobstructed view of the sky for the multi-antenna GPS attitude system which the performance of the presented algorithm would be compared against. The tests were preformed using a vehicle that underwent a series of pitch and roll dynamics to confirm the validity of the algorithm. Results shown in this section are those of the lidar attitude system when compared to a separate system, described in the following section, for determining vehicle attitude.

5.2.1 Hardware Overview

The vehicle used for the dynamic tests was an Infiniti G35 sedan. The same three-dimensional lidar presented in Section 3.1 was also used in these tests and data was recorded at 10Hz. It was mounted on the vehicle's roof-rack at a height of approximately 2m, and was roughly aligned to the vehicle yaw and roll axes, however there was a noticeable deviation between the pitch axes of the vehicle and the lidar of roughly 10°. This mounting was held constant throughout the tests. A Septentrio 3-antenna GPS receiver was used as a comparative system, which is capable of reporting the Euler angles of the vehicle's pitch, roll, and yaw. Data from which was also collected at 10Hz. The Septentrio system was accurate for the given baseline to within 0.6° [35]. It should be noted here that there was no elaborate calibration done on the Septentrio system to confirm that it was indeed mounted with perfect alignment to the vehicle's axes.

5.2.2 Test Procedure

Testing consisted of first calibrating the lidar to determine its initial pitch, roll and yaw on the vehicle. This was accomplished by have the vehicle first take static data, which consisted of simply taking fifty measurements of the parking garage roof while the vehicle was in park. The vehicle was then driven forward and the brakes applied abruptly to cause the vehicle to preform a pure pitch maneuver as previously described in Section 4.2. This pitched scan was then compared to the static data and the calibration parameters were calculated. The vehicle was then once again put in park, and it then underwent induced pitch and roll maneuvers, which consisted of one researcher jumping up and down on the bumper to induce pitch, and another researcher rocking the car side to side to induce roll. The reason dynamics were induced instead allowing them to occur naturally in a driving scenario were the following:

- It was not thought safe to preform high dynamic tests at this location.
- It was desired to keep environmental changes to a minimum
- This method appeared to assure sufficient dynamics which to test over.

5.2.3 Data Selection and Processing

Data from the lidar was taken from only Layers A and D over a range of 30° to 5° and -30° to -5°. Data was processed one scan at a time, and compared to the static data to determine vehicle dynamics. Data was once again split into three groups, group one consisted of data from Layer A over the range of 30° to 5°, group two consisted of data from Layer A over the range of -30° to -5°, and finally, group three consisted of data from layer D over the range of 30° to 5° and -30° to -5°. Hence, group three is twice as long as group one and two. In an effort to further reduce processing time, data was processed in such a way that the first element in group three was compared with the first element in groups one and two, the second element in group three, with the second in group one and two, and so on until groups one and two were exhausted. The data loop was then preformed again but starting with the first unprocessed data element in group three and the first element in groups one and two. Once attitude data was calculated, it was compared to the corresponding reading of the Septentrio system in an effort to determine system performance.

Table 5.1: Error Statistics Compared to Septentrio

MSE Pitch	0.1129°
MSE Roll	0.7855°
Avg Error Pitch	0.28°
Avg Error Roll	0.68°
Avg proc. time per scan	0.26s
Avg Calibration Time	66s

5.2.4 Dynamic Results

The results presented below are of the lidar attitude determination system when compared to a three-antenna Septentrio GPS receiver. Additionally, all data was post processed. It should be noted there is no metric presented to confirm the accuracy of the calibration phase. Instead, error presented in pitch and roll will simply show all errors occurred in the system. Results for the dynamic pitch and roll tests can be seen in Figures 5.5 and 5.6. Note that a slight over shoot over the lidar based system is present in both plots. A histogram of the error (difference) between the Septentrio and lidar system, can be seen in Figure 5.7. Finally Table 5.1, presented statistical data of the system's performance as well as processing times. Note that the calibration time is quite fast, and is thought to be reasonable for in the field calibration. Additionally, the processing time per scan give appears to be small enough for this system to be capable of being run real-time.

5.2.5 Skid Pad Testing

Finally, the results presented below are of the lidar attitude determination system when compared to a three-antenna Septentrio GPS receiver as presented in Section 5.2.4 while the vehicle underwent various driving maneuvers. The lidar was mounted similar to the mounting described in Section 5.2.1. The mounting of the lidar was calibrated by first simply scanning a portion of flat ground to determine the initial mounting pitch and roll. The pure pitch maneuver needed to ascertain the yaw between the lidar and the vehicle presented in Section

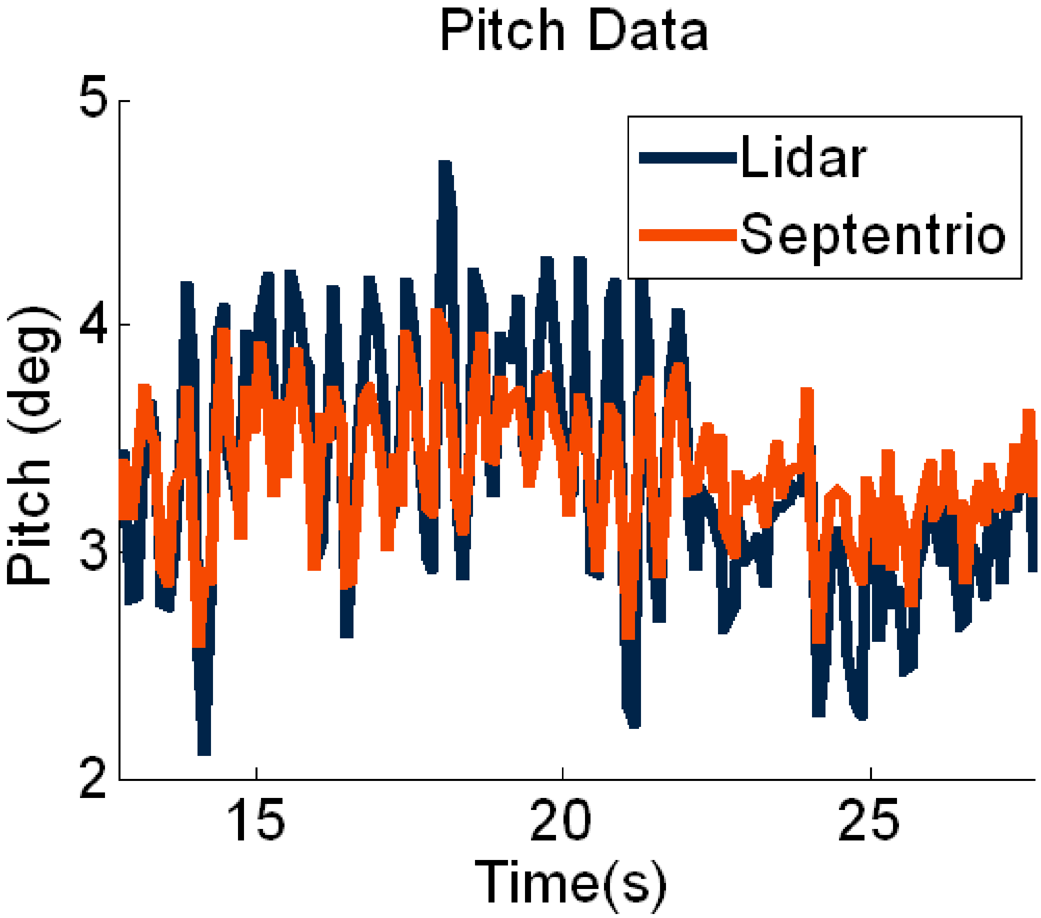

Figure 5.5: Lidar Method Pitch Compared to Septentrio Pitch

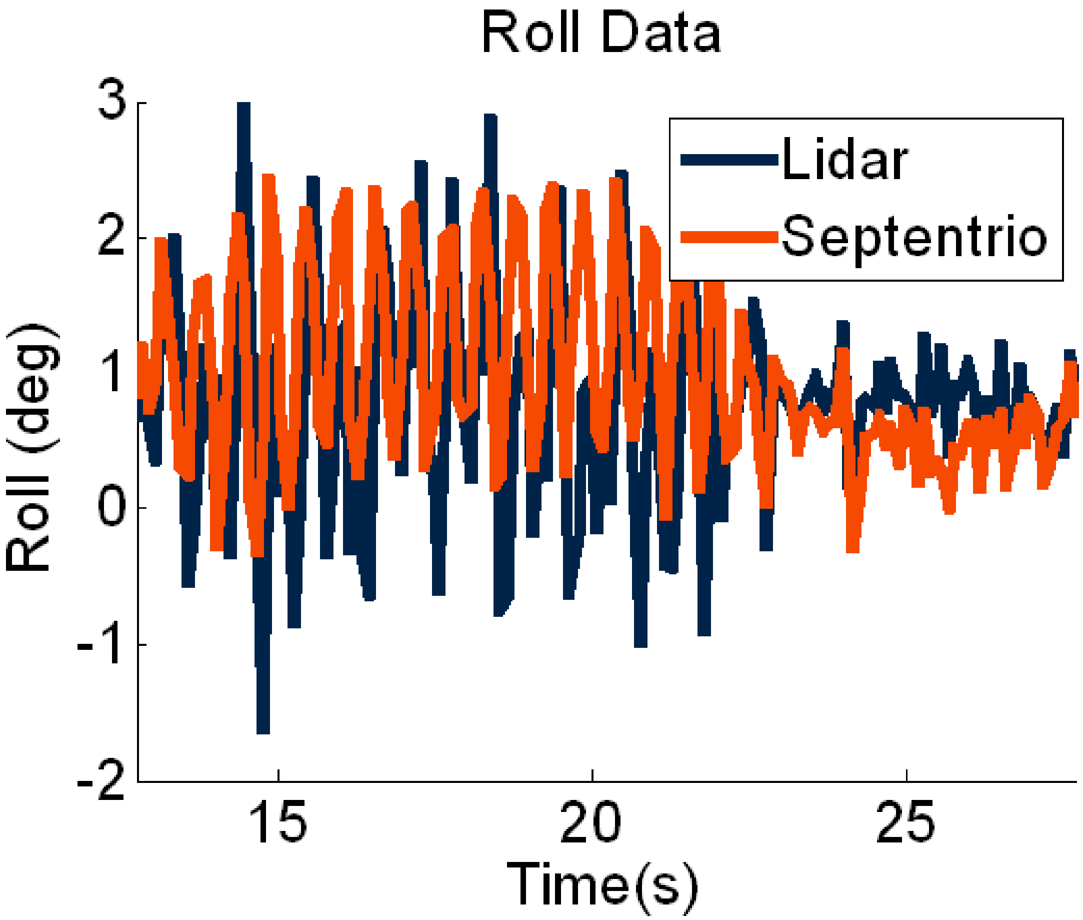

Figure 5.6: Lidar Method Roll Compared to Septentrio Roll

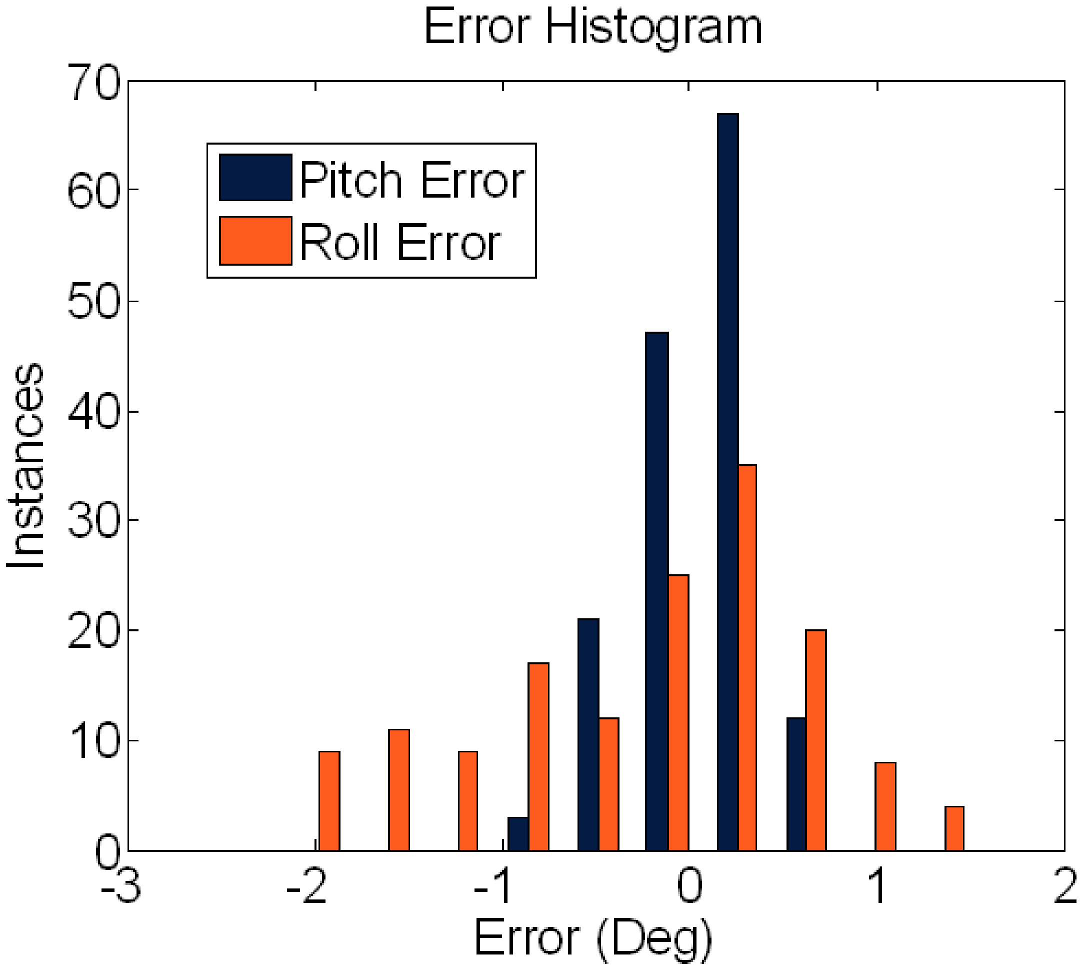

Figure 5.7: Difference Histogram

Table 5.2: Error Statistics Compared to Septentrio

MSE Pitch	2.054°
MSE Roll	0.4617°
Avg Error Pitch	0.79°
Avg Error Roll	0.31°
Avg proc. time per scan	0.05s
Avg Calibration Time	2.26s

4.2, was preformed by driving the car straight and abruptly applying the brakes. With all necessary calibration maneuvers preformed, the vehicle then underwent a series of dynamics to induce the vehicle to pitch and roll.

These maneuvers consisted of making a double lane change to induce roll while sharply throttling or braking the vehicle to induce pitch. The minimum and maximum pitch the vehicle experienced was -1.2548° and 2.9607°, with minimum and maximum roll of -2.5210° and 2.6700°, as reported by the Septentrio. Similarly, all data was post processed, however data was only processed between 10° to 5° and -10° to -5°, in an effort to further reduce processing time. It should be again noted there is no metric presented to confirm the accuracy of the calibration phase. Instead, errors presented in pitch and roll will simply show all errors occurred in the system. Data is presented only over the time span which the dynamics occur. Results for the dynamic pitch and roll tests can be seen in Figures 5.8 and 5.9. A histogram of the error (difference) between the Septentrio and lidar system, can be seen in Figure 5.10. Finally Table 5.2, presented statistical data of the system's performance as well as processing times. Note that the calibration time and processing time per scan is faster than those times presented in 5.1. This is due to the reduction in the angles which the data is processed over, and gives further credence to this algorithm being capable of preforming in real-time.

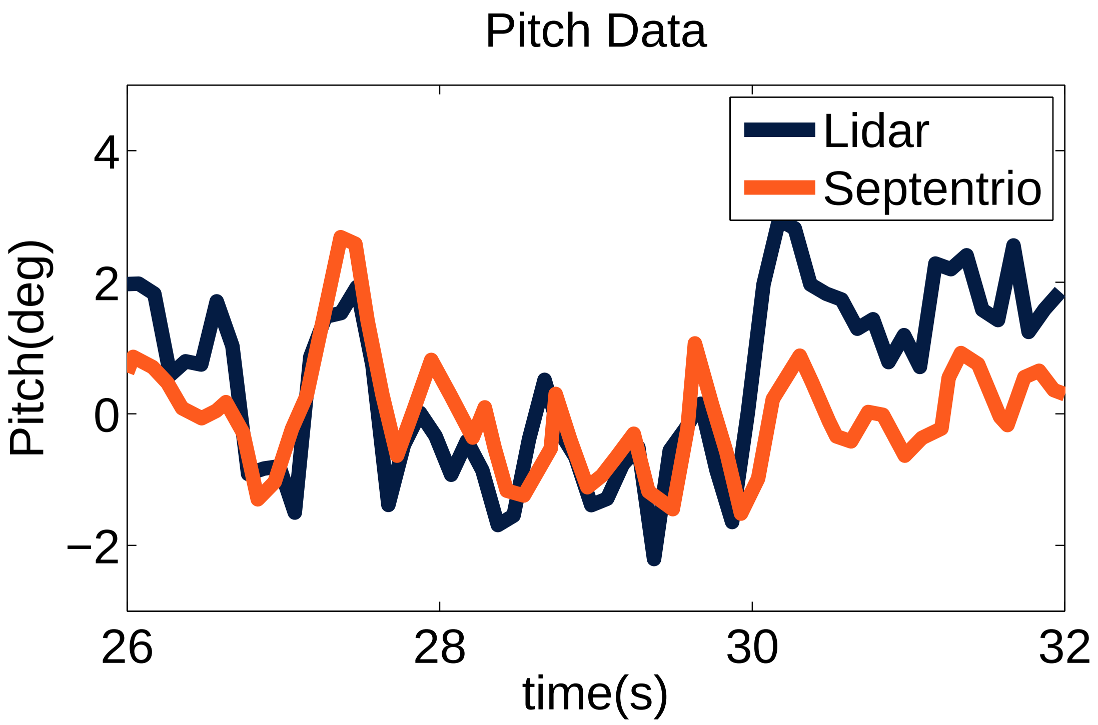

Figure 5.8: Lidar Method Pitch Compared to Septentrio Pitch

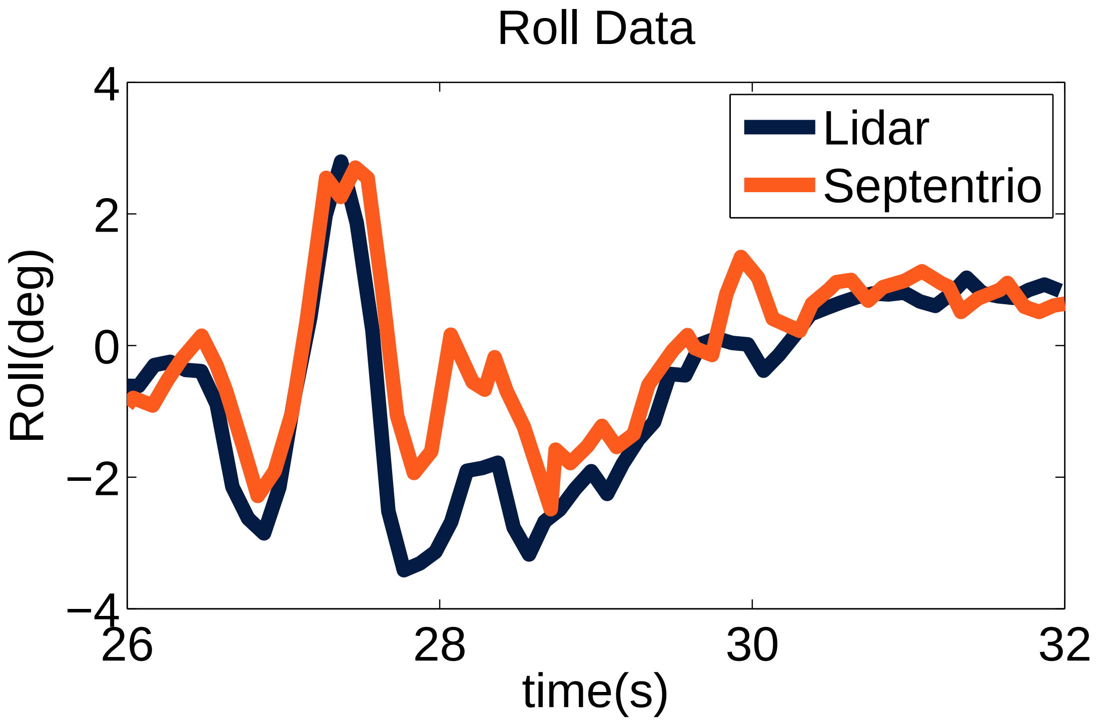

Figure 5.9: Lidar Method Roll Compared to Septentrio Roll

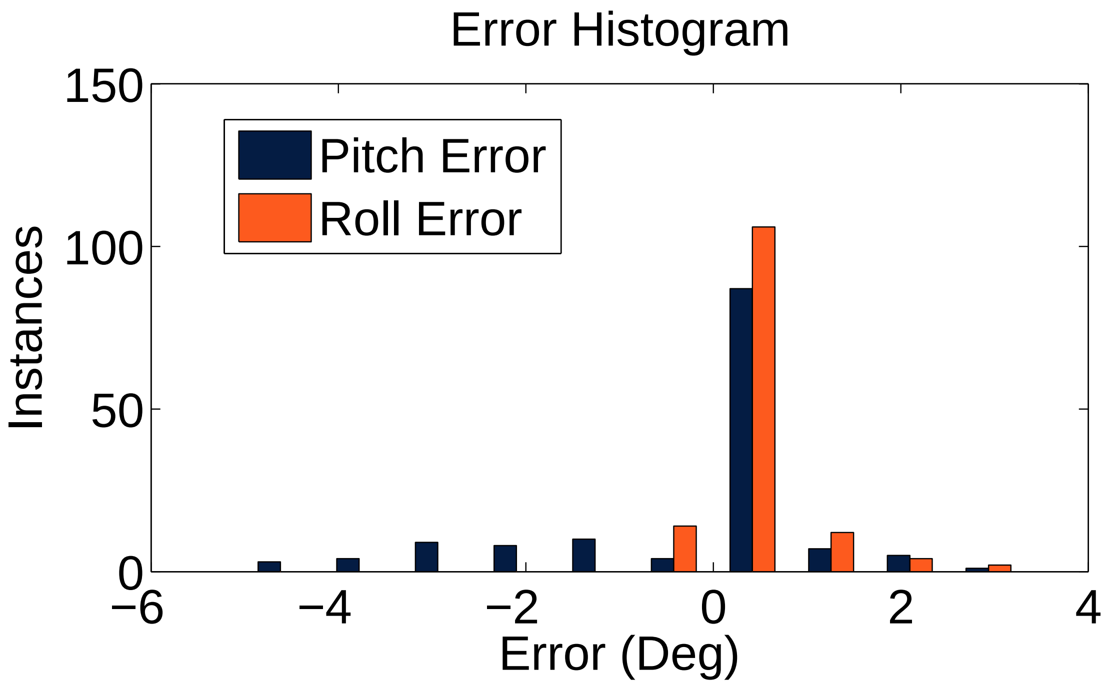

Figure 5.10: Difference Histogram

5.3 Conclusion and Future Work

This chapter has shown it is possible to determine the attitude of a vehicle using a 3D lidar to within sub degree accuracy. It should also be noted that the amount of data used to process the attitude will have significant affects on processing times, as noted in the difference between tables 5.2 and 5.1. It is also critical to be cable of preforming a pure pitch maneuver, which will allow the lidar to be properly aligned to the vehicle's axes. If the maneuver cannot be preformed properly, then the yaw between the lidar and vehicle can become incorrect and introduce errors in the measures of vehicle pitch and roll. Additionally, if the measuring surface is non-planar it is likely that this will induce errors in the attitude measurements. Future work should include real-time testing and potentially, blending this algorithm with an IMU so determine how accurately roll relative to a road can be distinguished from a global roll.

Chapter 6

Conclusions and Future Work

A lane marking detection method has been presented that attempts to generate the a model of an ideal lane's echo width , and then preform a best fit of that ideal lane to the lane the driver is currently driving on in an effort to ascertain the lateral position of the vehicle in the lane. A number of tests in highway scenarios have been presented of the algorithm using both the novel validation method of high accuracy RTK GPS as well as other means of testing currently employed in the field. From these tests it can be concluded that the algorithm is capable of detecting lane markings with over a 90% success rate to an accuracy of 0.075m. This algorithm has demonstrated its success at determining the vehicle's lateral position in that the average position error is less than that of a lane marker. Additionally, the presented algorithm is highly dynamic, allowing it to easily transition road types, conditions, and mounting locations.

Additionally, a novel lidar calibration and attitude determination algorithm has been presented. The algorithm has shown that all that is needed to calibrate a 3D forward facing lidar is a level plane and a pitch dynamic, as opposed to other more time consuming and tedious methods involving calibration devices, highly controlled maneuvers, or calibration targets, all the while doing so in a matter of seconds. The presented algorithm also has the ability to determine the vehicle's attitude once it has calibrated the lidar. Testing of the vehicle attitude determination algorithm was performed both in benign environments as well as skid pad testing, during which the test vehicle underwent highly dynamic maneuvers. Finally, from these tests, it has been shown that the attitude determination algorithm is capable of determining the vehicle's pitch and roll to within sub-degree accuracy, while doing so at a rate that is capable of running real-time.

6.1 Future Work

Future work for the lane detection algorithm should include testing in harsh environments so that performance of the lidar can be assessed quantitatively in situations where it might prove most valuable. Additional work should also attempt to leverage the lidar's ability to receive multiple reflections from a single measurement to increase the robustness of the algorithm to environmental effects.

Future work for the attitude determination algorithm should include integration with a stability control algorithm to assess what reduction in rollover is possible. Additional future work should also include further determination of the algorithms performance into how non-planar the calibrating surface can be to still yield accurate results. Specifically, it should be accessed how much road crown is acceptable to yield accurate measurements.

Bibliography

[1] *A Consistent, Debiased Method for Converting Between Polar and Cartesian Coordinate Systems*, 1997.

[2] *A lidar-based approach for near range lane detection*, June 2005.

[3] John W. Allen, Jordan H. Britt, Christopher J. Rose, and David M. Bevly. Intelligent multi-sensor measurements to enhance vehicle navigation and safety systems. *International Technical Meeting of the Institute of Navigation*, pages 74–83, 2009.

[4] American Society of Naval Engineers. *Visual Tracking and LIDAR Relative Positioning for Automated Launch and Recovery of an Unmanned Rotorcraft from Ships at Sea*, Annapolis, May 2008.

[5] Matthew Antone and Yuli Friedman. Fully automated laser range calibration.

[6] E.P. Baltsavias. Airborne laser scanning: Basic relations and formulas. *ISPRS Journal of Photogrammetry & Remote Sensing*, 54:199–214, 1999.

[7] Frank S. Barickman. Lane departure warning system research and test development. *Transportation Research Center Inc.*, (07-0495), 2007.

[8] Ivo Boniolo, Mara Tanelli, and Sergio M. Savaresi. Roll angle estimation in two-wheeled vehicles. *IEEE International Conference on Control Applications*, 17:31–36, September 2008.

[9] Jordan Britt, David Bevly, and John Hung. Lidar pose estimation for vehicle safety systems. *SAE World Congress*, 2010.

[10] Jordan Britt, David J. Broderick, David Bevly, and John Hung. Lidar attitude estimation for vehicle safety systems. *IEEE PLANS*, 2010.

[11] Jordan H. Britt and David M. Bevly. Lane tracking using multilayer laser scanner to enhance vehicle navigation and safety systems. *International Technical Meeting of the Institute of Navigation*, pages 629 – 634, 2009.

[12] Y.D. Chen and J. Ni. Dynamic calibration and compensation of a 3-d laser radar scanning system. *IEEE Transactions on Robotics and Automation*, 9:318–323, 1993.

[13] K. Dietmayer, N. Kämpchen, K. Fürstenberg, J. Kibbel, W. Justus, and R. Schulz. *Advanced Microsystems for Automotive Applications 2005*. VDI-Buch. Springer Berlin Heidelberg, 2005.

[14] B. Fardi, H. Weigel, G. Wanielik, and K. Takagi. Road border recognition using fir images and lidar signal processing. In *Proc. IEEE Intelligent Vehicles Symposium*, pages 1278–1283, June 13–15, 2007.

[15] Jerry Ginsberg. *Engineering Dynamics*. Cambridge University Press, 2008.

[16] Mohinder S. Grewal, Lawrence R. Weill, and Angus P. Andrews. *Global Positioning Systems, Inertial Navigation, and Integration*. Wiley-Interscience, 2001.

[17] Aleksander Hac, Todd Brown, and John Martens. Detection of vehicle rollover. *SAE World Congress*, (2004-01-1757), March 2004.

[18] Dr. R. Schulz T. Kluge J. Scholz, V. Willhoeft. *ALASCA User Manual*. Ibeo Automobile Sensor GmbH, Fahrenkron 125 22179 Hamburg Germany, 2.0.0 edition, February 2006.

[19] Bjorn Johannson and Magnus Gafvert. Untripped suv rollover detection and prevention. *IEEE Conference on Decision and Control*, 43:5461–5466, December 2004.

[20] Simon J. Julier. The spherical simplex unscented transformation. *American Control Conference*, pages 2430–2434, June 2003.

[21] Jongchul Jung, Taehyun Shim, and Jamie Gertsch. A vehicle roll-stability indicator incorporating roll-center movements. *IEEE Transactions on Vehicular Technology*, 58:4078–4087, October 2009.

[22] S. Kammel and B. Pitzer. Lidar-based lane marker detection and mapping. In *Proc. IEEE Intelligent Vehicles Symposium*, pages 1137–1142, June 4–6, 2008.

[23] J. Kibbel, W. Justus, and K. Furstenberg. Lane estimation and departure warning using multilayer laserscanner. In *Proc. IEEE Intelligent Transportation Systems*, pages 607–611, September 13–15, 2005.

[24] P. Lindner, E. Richter, G. Wanielik, K. Takagi, and A. Isogai. Multi-channel lidar processing for lane detection and estimation. In *Proc. 12th International IEEE Conference on Intelligent Transportation Systems ITSC '09*, pages 1–6, October 4–7, 2009.

[25] United States Department of Transportation Federal Highway Administration. Roadway departure safety. Online, January 2010.

[26] T. Ogawa and K. Takagi. Lane recognition using on-vehicle lidar. In *Proc. IEEE Intelligent Vehicles Symposium*, pages 540–545, 2006.

[27] A. Pothou, C. Toth, S. Karamitsos, and A. Georgopoulos. On using qa/qc techniques for lidar-imu boresight misalignment. *International Symposium on Mobile Mapping Technology*, 5, 2007.

[28] Guo qing Wei and Gerd Hirzinger. Active self-calibration of hand-mounted laser range finders. *IEEE Trans. Robotics and Automation*, 14:493–497, 1998.

[29] Christopher Rose and David M. Bevly. Vehicle lane position estimation with camera vision using bounded polynomial interpolated lines. *International Technical Meeting of the Institute of Navigation*, pages 102 – 108, 2009.

[30] Solmaz S., Akar M., and Shorten R. Center of gravity estimation and rollover prevention using multiple models & controllers. *Yale workshop on adaptive & learning systems*, 14:177–183, June 2008.

[31] Solmaz S., Corless M., and Shorten R. A methodology for the design of robust rollover prevention controllers for automotive vehicles: Part 2-active steering. *American Control Conference*, pages 1606–1611, July 2007.

[32] Davide Scaramuzza, Ahad Harati, and Roland Siegwart. Extrinsic self calibration of a camera and a 3d laser range finder from natural scenes. pages 4164–4169, 2007.

[33] J.K Schiffmann. Vehicle rollover sensing using short-term integration, 2000.

[34] Clugg C. A. Schubert, P.J. Adaptive rollover detection apparatus and method, 2003.

[35] Septentrio Satellive Navigation, Ubicenter, Philipssite 5, B-3001 Leuven, Belgium. *PolaRx2/2e User Mannual*, 3.2.0 edition, January 2007.

[36] James Bao-Yen Tsui. *Fundamentals of Global Positioning System Recievers*. Wiley-Interscience, 2000.

[37] Toshihiro Tsumura, Hiroshi Okubo, and Nobuo Komatsu. A 3-d position and attitude measurement system using laser scanners and corner cubes. *IEEE/RSJ International Conference on Intelligent Robots and Systems*, pages 604–611, 1993.

[38] Zhenqi Zhu, Qing Tang, Jinsong Li, and Zhongxue Gan. Calibration of laser displacement sensor used by industrial robots. *Optical Engineering*, 43(1):12–13, 2004.

Appendices

Appendix A

Rotation Matrix Expansions

$$
\begin{bmatrix} N_i \\ E_i \\ D_i \end{bmatrix} = \begin{bmatrix} \cos(\lambda) & 0 & -\sin(\lambda) \\ 0 & 1 & 0 \\ \sin(\lambda) & 0 & \cos(\lambda) \end{bmatrix} \begin{bmatrix} 1 & 0 & 0 \\ 0 & \cos(\zeta) & \sin(\zeta) \\ 0 & -\sin(\zeta) & \cos(\zeta) \end{bmatrix}
\left(\begin{bmatrix} 1 & 0 & 0 \\ 0 & \cos(\phi) & \sin(\phi) \\ 0 & -\sin(\phi) & \cos(\phi) \end{bmatrix} \begin{bmatrix} \cos(\theta) & 0 & -\sin(\theta) \\ 0 & 1 & 0 \\ \sin(\theta) & 0 & \cos(\theta) \end{bmatrix} \begin{bmatrix} \cos(\psi) & \sin(\psi) & 0 \\ -\sin(\psi) & \cos(\psi) & 0 \\ 0 & 0 & 1 \end{bmatrix} \right)^{\intercal} \begin{bmatrix} x_i \\ y_i \\ z_i \end{bmatrix} \tag{A.1}
$$

Expanding D_i :

$$
\begin{gathered}
D_i = \sin(\lambda)((\sin(\psi)\,(-z_i \sin(\phi) + y_i \cos(\phi)) \\
+ \cos(\psi)\,(-x_i \cos(\theta) - y_i \sin(\phi) \sin(\theta) - z_i \cos(\phi) \sin(\theta))) \\
+ \cos(\lambda)(\sin(\zeta)(y_i \sin(\phi) sin(\theta) \sin(\psi) + x_i \cos(\theta) \sin(\psi) \\
+ y_i cos(\phi) \cos(\psi) + z_i \cos(\phi) \sin(\theta) \sin(\psi) - z_i \sin(\phi) cos(\psi)) \\
+ \cos(\zeta)\,(y_i \sin(\phi) cos(\theta) - x_i \sin(\theta) + z_i \cos(\phi) \cos(\theta)))
\end{gathered} \tag{A.2}
$$

Solving for the scan coordinates in the lidar frame:

$$
NED_{lidar\,frame} =
\left(\begin{bmatrix} 1 & 0 & 0 \\ 0 & \cos(\phi) & \sin(\phi) \\ 0 & -\sin(\phi) & \cos(\phi) \end{bmatrix} \begin{bmatrix} \cos(\theta) & 0 & -\sin(\theta) \\ 0 & 1 & 0 \\ \sin(\theta) & 0 & \cos(\theta) \end{bmatrix} \begin{bmatrix} \cos(\psi) & \sin(\psi) & 0 \\ -\sin(\psi) & \cos(\psi) & 0 \\ 0 & 0 & 1 \end{bmatrix} \right)^{\intercal} \begin{bmatrix} x_i \\ y_i \\ z_i \end{bmatrix} \tag{A.3}
$$

$D_{lidar\,frame}$expanded:

$$h_j = -\sin(\theta)x_j + \sin(\phi)\cos(\theta)y_j + \cos(\phi)\cos(\theta)z_j \tag{A.4}$$

Beginning with at least three instances of equation A.4:

$$h_1 = -\sin(\theta)x_1 + \sin(\phi)\cos(\theta)y_1 + \cos(\phi)\cos(\theta)z_1 \tag{A.5}$$

$$h_2 = -\sin(\theta)x_2 + \sin(\phi)\cos(\theta)y_2 + \cos(\phi)\cos(\theta)z_2 \tag{A.6}$$

$$h_3 = -\sin(\theta)x_3 + \sin(\phi)\cos(\theta)y_3 + \cos(\phi)\cos(\theta)z_3 \tag{A.7}$$

Setting equations A.5 and A.6 equal to one another yields:

$$\begin{gathered} -\sin(\theta)x_1 + \sin(\phi)\cos(\theta)y_1 + \cos(\phi)\cos(\theta)z_1 \\ = -\sin(\theta)x_2 + \sin(\phi)\cos(\theta)y_2 + \cos(\phi)\cos(\theta)z_2 \end{gathered} \tag{A.8}$$

Putting similar trig identities involving θ terms on same side of the equals sign yields:

$$\begin{gathered} \sin(\theta)x_2 - \sin(\theta)x_1 \\ = \sin(\phi)\cos(\theta)y_2 + \cos(\phi)\cos(\theta)z_2 + \sin(\phi)\cos(\theta)y_1 + \cos(\phi)\cos(\theta)z_1 \end{gathered} \tag{A.9}$$

Collecting like trig terms involving θ:

$$\sin(\theta)(x_2 - x_1) = \cos(\theta)\left(\sin(\phi)y_2 + \cos(\phi)z_2 + \sin(\phi)y_1 + \cos(\phi)z_1\right) \tag{A.10}$$

Dividing through by $\cos(\theta)$ and solving for theta yields:

$$\theta_{12} = \arctan\left(\frac{\sin(\phi)y_2 + \cos(\phi)z_2 - \sin(\phi)y_1 - \cos(\phi)z_1}{(x_2 - x_1)}\right) \tag{A.11}$$

Collecting like terms:

$$\theta_{12} = \arctan\left(\frac{\sin(\phi)(y_2 - y_1) + \cos(\phi)(z_2 - z_1)}{(x_2 - x_1)}\right) \tag{A.12}$$

Hence:

$$\theta_{13} = \arctan\left(\frac{\sin(\phi)(y_3 - y_1) + \cos(\phi)(z_3 - z_1)}{(x_3 - x_1)}\right) \tag{A.13}$$

$$\theta_{32} = \arctan\left(\frac{\sin(\phi)(y_2 - y_3) + \cos(\phi)(z_2 - z_3)}{(x_2 - x_3)}\right) \tag{A.14}$$

Roll can be found by setting equations A.12 and A.13 equal to one another:

$$\begin{gathered}\arctan\left(\tfrac{\sin(\phi)(y_2-y_1)+\cos(\phi)(z_2-z_1)}{(x_2-x_1)}\right)\\ = \arctan\left(\tfrac{\sin(\phi)(y_3-y_1)+\cos(\phi)(z_3-z_1)}{(x_3-x_1)}\right)\end{gathered} \tag{A.15}$$

Canceling out arctan terms and cross-multiplying:

$$\begin{gathered}\left(\sin(\phi)(y_2 - y_1) + \cos(\phi)(z_2 - z_1)\right)(x_3 - x_1)\\ = \left(\sin(\phi)(y_3 - y_1) + \cos(\phi)(z_3 - z_1)\right)(x_2 - x_1)\end{gathered} \tag{A.16}$$

Expanding:

$$\begin{gathered}\sin(\phi)(y_2 - y_1)(x_3 - x_1) + \cos(\phi)(z_2 - z_1)(x_3 - x_1)\\ = \sin(\phi)(y_3 - y_1)(x_2 - x_1) + \cos(\phi)(z_3 - z_1)(x_2 - x_1)\end{gathered} \tag{A.17}$$

Putting similar trig terms on same side of equals sign and grouping like terms:

$$\begin{gathered}\sin(\phi)\left((y_2 - y_1)(x_3 - x_1) - (y_3 - y_1)(x_2 - x_1)\right)\\ = \cos(\phi)\left((z_3 - z_1)(x_2 - x_1) - (z_2 - z_1)(x_3 - x_1)\right)\end{gathered} \tag{A.18}$$

Dividing through by $\cos(\phi)$ and solving for ϕ.

$$\phi = \arctan\left(\frac{((z_3 - z_1)(x_2 - x_1) - (z_2 - z_1)(x_3 - x_1))}{((y_2 - y_1)(x_3 - x_1) - (y_3 - y_1)(x_2 - x_1))}\right) \tag{A.19}$$

Appendix B

Determining Vehicle Frame Pitch Calculations

Beginning with three instances of equation A.2.

$$\begin{gathered}
D_1 = \sin(\lambda)((\sin(\psi)\left(-z_1 \sin(\phi) + y_1 \cos(\phi)\right) \\
+ \cos(\psi)\left(-x_1 \cos(\theta) - y_1 \sin(\phi) \sin(\theta) - z_1 \cos(\phi) \sin(\theta)\right)) \\
+ \cos(\lambda)(\sin(\zeta)(y_1 \sin(\phi) sin(\theta) \sin(\psi) + x_1 \cos(\theta) \sin(\psi) \\
+ y_1 cos(\phi) \cos(\psi) + z_1 \cos(\phi) \sin(\theta) \sin(\psi) - z_1 \sin(\phi) cos(\psi)) \\
+ \cos(\zeta)\left(y_1 \sin(\phi) cos(\theta) - x_1 \sin(\theta) + z_1 \cos(\phi) \cos(\theta)\right))
\end{gathered} \tag{B.1}$$

$$\begin{gathered}
D_2 = \sin(\lambda)((\sin(\psi)\left(-z_2 \sin(\phi) + y_2 \cos(\phi)\right) \\
+ \cos(\psi)\left(-x_2 \cos(\theta) - y_2 \sin(\phi) \sin(\theta) - z_2 \cos(\phi) \sin(\theta)\right)) \\
+ \cos(\lambda)(\sin(\zeta)(y_2 \sin(\phi) sin(\theta) \sin(\psi) + x_2 \cos(\theta) \sin(\psi) \\
+ y_2 cos(\phi) \cos(\psi) + z_2 \cos(\phi) \sin(\theta) \sin(\psi) - z_2 \sin(\phi) cos(\psi)) \\
+ \cos(\zeta)\left(y_2 \sin(\phi) cos(\theta) - x_2 \sin(\theta) + z_2 \cos(\phi) \cos(\theta)\right))
\end{gathered} \tag{B.2}$$

$$\begin{gathered}
D_3 = \sin(\lambda)((\sin(\psi)\left(-z_3 \sin(\phi) + y_i \cos(\phi)\right) \\
+ \cos(\psi)\left(-x_3 \cos(\theta) - y_3 \sin(\phi) \sin(\theta) - z_3 \cos(\phi) \sin(\theta)\right)) \\
+ \cos(\lambda)(\sin(\zeta)(y_3 \sin(\phi) sin(\theta) \sin(\psi) + x_3 \cos(\theta) \sin(\psi) \\
+ y_3 cos(\phi) \cos(\psi) + z_3 \cos(\phi) \sin(\theta) \sin(\psi) - z_3 \sin(\phi) cos(\psi)) \\
+ \cos(\zeta)\left(y_3 \sin(\phi) cos(\theta) - x_3 \sin(\theta) + z_3 \cos(\phi) \cos(\theta)\right))
\end{gathered} \tag{B.3}$$

The following constants are defined to simplify the above equations.

$$\begin{gathered}
A_1 = -y_1 \sin(\phi) \cos(\theta) + x_1 \sin(\theta) - z_1 \cos(\phi) \cos(\theta) \\
+ z_2 \cos(\phi) \cos(\theta) + y_2 \sin(\phi) \cos(\theta) - x_2 \sin(\theta)
\end{gathered} \tag{B.4}$$

$$\begin{aligned} B_1 = {} & y_3\sin(\phi)\cos(\theta) - x_3\sin(\theta) + z_3\cos(\phi)\cos(\theta) \\ & -y_1\sin(\phi)\cos(\theta) + x_1\sin(\theta) - z_1\cos(\phi)\cos(\theta) \end{aligned} \tag{B.5}$$

$$\begin{aligned} C_1 = {} & -y_2\sin(\phi)\cos(\theta) + x_2\sin(\theta) - z_2\cos(\phi)\cos(\theta) \\ & +z_3\cos(\phi)\cos(\theta) + y_3\sin(\phi)\cos(\theta) - x_3\sin(\theta) \end{aligned} \tag{B.6}$$

$$D_1 = -z_2\sin(\phi) + y_2\cos(\phi) + z_1\sin(\phi) - y_1\cos(\phi) \tag{B.7}$$

$$E_1 = (-z_3\sin(\phi) + z_1\sin(\phi) + y_3\cos(\phi) - y_1\cos(\phi)) \tag{B.8}$$

$$F_1 = (-z_3\sin(\phi) + z_2\sin(\phi) + y_3\cos(\phi) - y_2\cos(\phi)) \tag{B.9}$$

$$\begin{aligned} G_1 = {} & (-x_1\cos(\theta) + z_2\cos(\phi)\sin(\theta) - y_1\sin(\phi)\sin(\theta) \\ & +y_2\sin(\phi)\sin(\theta) + x_2\cos(\theta) - z_1\cos(\phi)\sin(\theta)) \end{aligned} \tag{B.10}$$

$$\begin{aligned} H_1 = {} & (z_3\cos(\phi)\sin(\theta) + y_3\sin(\phi)\sin(\theta) + x_3\cos(\theta) \\ & -z_1\cos(\phi)\sin(\theta) - y_1\sin(\phi)\sin(\theta) - x_1\cos(\theta)) \end{aligned} \tag{B.11}$$

$$\begin{aligned} I_1 = {} & (y_3\sin(\phi)\sin(\theta) + x_3\cos(\theta) - x_2\cos(\theta) \\ & +z_3\cos(\phi)\sin(\theta) - z_2\cos(\phi)\sin(\theta) - y_2\sin(\phi)\sin(\theta)) \end{aligned} \tag{B.12}$$

Setting equations B.1 and B.2 equal to one another and simplifying yields:

$$\lambda_{12} = \arctan\left(\frac{\cos(\zeta)A_1 + \sin(\zeta)\left(\cos(\psi)D_1 + \sin(\psi)G_1\right)}{\cos(\psi)G_1 - \sin(\psi)D_1}\right) \tag{B.13}$$

Setting equations B.1 and B.3 equal to one another and simplifying yields:

$$\lambda_{13} = \arctan\left(\frac{\cos(\zeta)B_1 + \sin(\zeta)\left(\cos(\psi)E_1 + \sin(\psi)H_1\right)}{\cos(\psi)H_1 - \sin(\psi)E_1}\right) \tag{B.14}$$

Appendix C

Determining Vehicle Frame Pitch Dynamic Calculations

The following constants are defined to simplify the above equations.

$$\begin{aligned}A_{11} &= -y_{11}\sin(\phi)\cos(\theta) + x_{11}\sin(\theta) - z_{11}\cos(\phi)\cos(\theta)\\ &+z_{22}\cos(\phi)\cos(\theta) + y_{22}\sin(\phi)\cos(\theta) - x_{22}\sin(\theta)\end{aligned} \tag{C.1}$$

$$\begin{aligned}B_{11} &= y_{33}\sin(\phi)\cos(\theta) - x_{33}\sin(\theta) + z_{33}\cos(\phi)\cos(\theta)\\ &-y_{11}\sin(\phi)\cos(\theta) + x_{11}\sin(\theta) - z_{11}\cos(\phi)\cos(\theta)\end{aligned} \tag{C.2}$$

$$\begin{aligned}C_{11} &= -y_{22}\sin(\phi)\cos(\theta) + x_{22}\sin(\theta) - z_{22}\cos(\phi)\cos(\theta)\\ &+z_{33}\cos(\phi)\cos(\theta) + y_{33}\sin(\phi)\cos(\theta) - x_{33}\sin(\theta)\end{aligned} \tag{C.3}$$

$$D_{11} = -z_{22}\sin(\phi) + y_{22}\cos(\phi) + z_{11}\sin(\phi) - y_{11}\cos(\phi) \tag{C.4}$$

$$E_{11} = (-z_{33}\sin(\phi) + z_{11}\sin(\phi) + y_{33}\cos(\phi) - y_{11}\cos(\phi)) \tag{C.5}$$

$$F_{11} = (-z_{33}\sin(\phi) + z_{22}\sin(\phi) + y_{33}\cos(\phi) - y_{22}\cos(\phi)) \tag{C.6}$$

$$\begin{aligned}G_{11} &= (-x_{11}\cos(\theta) + z_{22}\cos(\phi)\sin(\theta) - y_{11}\sin(\phi)\sin(\theta)\\ &+y_{22}\sin(\phi)\sin(\theta) + x_{22}\cos(\theta) - z_{11}\cos(\phi)\sin(\theta))\end{aligned} \tag{C.7}$$

$$\begin{aligned}H_{11} &= (z_{33}\cos(\phi)\sin(\theta) + y_{33}\sin(\phi)\sin(\theta) + x_{33}\cos(\theta)\\ &-z_{11}\cos(\phi)\sin(\theta) - y_{11}\sin(\phi)\sin(\theta) - x_{11}\cos(\theta))\end{aligned} \tag{C.8}$$

$$
\begin{aligned}
I_{11} = (&y_{33}\sin(\phi)\sin(\theta) + x_{33}\cos(\theta) - x_{22}\cos(\theta) \\
&+z_{33}\cos(\phi)\sin(\theta) - z_{22}\cos(\phi)\sin(\theta) - y_{22}\sin(\phi)\sin(\theta))
\end{aligned}
\tag{C.9}
$$

Setting equations B.1 and B.2 equal to one another and simplifying yields:

$$\lambda_{1122} = \arctan\left(\frac{\cos(\zeta)A_{11} + \sin(\zeta)\left(\cos(\psi)D_{11} + \sin(\psi)G_{11}\right)}{\cos(\psi)G_{11} - \sin(\psi)D_{11}}\right) \tag{C.10}$$

Setting equations B.1 and B.3 equal to one another and simplifying yields:

$$\lambda_{1133} = \arctan\left(\frac{\cos(\zeta)B_{11} + \sin(\zeta)\left(\cos(\psi)E_{11} + \sin(\psi)H_{11}\right)}{\cos(\psi)H_{11} - \sin(\psi)E_{11}}\right) \tag{C.11}$$

Appendix D

Determining Vehicle Frame Roll Dynamic Calculations

Setting equation B.13 and B.14 equal to one another yields:

$$\begin{gathered}\arctan\left(\tfrac{\cos(\zeta)A_1+\sin(\zeta)(\cos(\psi)D_1+\sin(\psi)G_1)}{\cos(\psi)G_1-\sin(\psi)D_1}\right)\\ =\arctan\left(\tfrac{\cos(\zeta)B_1+\sin(\zeta)(\cos(\psi)E_1+\sin(\psi)H_1)}{\cos(\psi)H_1-\sin(\psi)E_1}\right)\end{gathered} \tag{D.1}$$

Simplifying Equation D.3 yields:

$$\zeta_{1213}=\arctan\left(\frac{\cos(\psi)(B_1G_1-A_1H_1)+\sin(\psi)(-B_1D_1+A_1E_1)}{D_1H_1-E_1G_1}\right) \tag{D.2}$$

Setting equation C.10 and C.11 equal to one another yields:

$$\begin{gathered}\arctan\left(\tfrac{\cos(\zeta)A_{11}+\sin(\zeta)(\cos(\psi)D_{11}+\sin(\psi)G_{11})}{\cos(\psi)G_{11}-\sin(\psi)D_{11}}\right)\\ =\arctan\left(\tfrac{\cos(\zeta)B_{11}+\sin(\zeta)(\cos(\psi)E_{11}+\sin(\psi)H_{11})}{\cos(\psi)H_{11}-\sin(\psi)E_{11}}\right)\end{gathered} \tag{D.3}$$

Simplifying Equation D.3 yields:

$$\zeta_{11221133}=\arctan\left(\frac{\cos(\psi)(B_{11}G_{11}-A_{11}H_{11})+\sin(\psi)(-B_{11}D_{11}+A_{11}E_{11})}{D_{11}H_{11}-E_{11}G_{11}}\right) \tag{D.4}$$

Appendix E

Yaw Offset Calculations

Setting equations D.2and D.4 equal to one another yields:

$$\begin{aligned}&\arctan\left(\frac{\cos(\psi)(B_1G_1-A_1H_1)+\sin(\psi)(-B_1D_1+A_1E_1)}{D_1H_1-E_1G_1}\right)\\&=\arctan\left(\frac{\cos(\psi)(B_{11}G_{11}-A_{11}H_{11})+\sin(\psi)(-B_{11}D_{11}+A_{11}E_{11})}{D_{11}H_{11}-E_{11}G_{11}}\right)\end{aligned} \tag{E.1}$$

Simplifying equation E.1 yields:

$$\psi=\arctan\left(\frac{(B_{11}G_{11}-A_{11}H_{11})(D_1H_1-E_1G_1)-(B_1G_1-A_1H_1)(D_{11}H_{11}-E_{11}G_{11})}{(-B_1D_1+A_1E_1)(D_{11}H_{11}-E_{11}G_{11})-(-B_{11}D_{11}+A_{11}E_{11})(D_1H_1-E_1G_1)}\right) \tag{E.2}$$